

Studies on a protein-protein interaction in the bacterial magnetic organelle “magnetosome”

メタデータ	言語: eng 出版者: 公開日: 2017-10-05 キーワード (Ja): キーワード (En): 作成者: メールアドレス: 所属:
URL	http://hdl.handle.net/2297/46593

This work is licensed under a Creative Commons Attribution-NonCommercial-ShareAlike 3.0 International License.



Dissertation

Studies on a protein-protein interaction in the bacterial magnetic organelle “magnetosome”

細菌の磁気オルガネラ「マグネトソーム」におけるタ
ンパク質間相互作用に関する研究

Graduate School of
Natural Science and Technology
Kanazawa University

Division of Life Science

Student ID: 1323032005

Name: Nguyen Viet Hoang

Chief advisor: Hiroshi Endoh

Advisor: Yoshihiro Fukumori

Date of Submission: 30th June 2016

CONTENTS

Abbreviations		2
Chapter I	General introduction	3
	References	9
	Figures	13
Chapter II	A protein-protein interaction in magnetosome: TPR protein MamA interacts with magnetite biomineralizing protein Mms6	
	Introduction	20
	Materials and Methods	22
	Results and Discussion	29
	References	33
	Figures and Tables	35
Chapter III	Identification of MamA binding site in Mms6	
	Introduction	52
	Materials and Methods	54
	Results and Discussion	57
	References	62
	Figures and Tables	65
Conclusions		82
Acknowledgements		83

Abbreviations

ATCC	American Type Culture Collection
MTB	magnetotactic bacteria
TPR	tetratricopeptide repeat
MAI	magnetosome island
A ₆₀₀	absorbance at 600 nm
SDS PAGE	sodium dodecyl surface polyacrylamide gel electrophoresis
kDa	kilo Dalton or 1,000 dalton
$\Delta mamA$	<i>mamA</i> deletion mutant
$\Delta mms6$	<i>mms6</i> deletion mutant
LB medium	Luria-Bertani medium
IgG	immunoglobulin G
a. a.	amino acid
Mms6 ¹⁻¹³³	full length Mms6 peptide with amino acids 1 to 133
Mms6 ¹⁻¹¹¹	Mms6 peptide with amino acids from 1 to 111
Mms6 ¹⁻⁸⁸	Mms6 peptide with amino acids from 1 to 88
Mms6 ⁷⁵⁻¹³³	Mms6 peptide with amino acids from 75 to 133
PCR	polymerise chain reaction
IPTG	isopropyl- β -D-thiogalactopyranoside
SEC	size exclusion chromatography
CHAPS	3-[(3-cholamidopropyl)dimethylammonio]-1-propanesulfonate

Chapter I

General Introduction

For many years ago, bacteria were thought as the “bags of enzymes”, however, due to the development of electron microscopy, bacterial structures have been studied well. Interestingly, many bacteria were recently investigated to contain intracellular macromolecular compartments which have order structures and specific components that are similar to eukaryotic counterparts. The compartments are referred to as bacterial organelles (1, 2). There is considerable interest in how such complex organelles form in bacteria. However, the study on bacterial organelles has a short history, therefore the understanding of them is limited to the comparison to eukaryotic organelles. Bacterial organelles can be divided into two classes. One class is bounded by a proteinaceous layer, e.g. carboxysomes (3) and gas vesicles (4), while the other class is surrounded by a lipid-bilayer membrane, e.g. pirellulosomes (5). Recent researches have focused on the proteinaceous-type of organelles due to their important roles in metabolic activities, e.g. the CO₂ fixation in the carboxysome (6-8). On the other hand, a little progress has been made about the lipid-bilayer class which is similar to eukaryotic organelles. A well-known example of membrane-enveloped bacterial organelles is magnetosomes, which are found in magnetotactic bacteria (MTB) (9-11). The magnetosomes allow MTB to align and swim along the geomagnetic field when MTB move to find a favorable microaerobic habitat (9-11).

MTB are a diverse group of aquatic bacteria which are found in sediments of freshwater, marine and hypersaline habitats (12). The phylogenetic diversity of MTB is belonging to *Alpha-*, *Gamma-*, *Delta-proteobacteria* classes of the *Proteobacterium* phylum, or the *Nitrospira* phylum, or the candidate division *Omnitrophica* (OP3) phylum according to 16S rRNA sequences. MTB contain magnetosomes, which consisted of nano-sized magnetic crystals, magnetite (Fe₃O₄) or greigite (Fe₃S₄), that

function as a magnetic sensor for bacterial orientation following the geomagnetic field.

The detailed process of magnetosome formation is still not clearly understood. However, I introduce here a recent model about the magnetosome formation (13) (Fig. 1-1). First, magnetosome vesicles are formed by invaginations of the cytoplasmic membrane. Second, the individual vesicles are assembled into a chain. Finally, iron ions are transferred into the magnetosome vesicles from cytoplasm using magnetosome specific iron transporters (14), then magnetite crystals are mineralized in the vesicles (13) (Fig. 1-1). Each of the steps is mediated by a specific set of magnetosome-associated proteins. Most of magnetosome-associated proteins are encoded from *mam* (magnetosome membrane) or *mms* (magnetite particle membrane specific) genes in the MTB specific genomic region, termed the magnetosome island (MAI) (15-18) (Fig. 1-2). At present, 13 MAI sequences have been revealed from phylogenetically diverse MTB belonging to the *Alpha*-, *Gamma*-, *Delta*-*proteobacteria*, and *Nitrospirae* (19).

Magnetospirillum magneticum AMB-1 belonging to *alphaproteobacteria* is one of the most studied MTB. AMB-1 is now used as a model species of MTB because AMB-1 is purely cultivated and is the most widely used strain in genetic and molecular techniques of MTB studies. In *M. magneticum* AMB-1, magnetosome-associated proteins are encoded in the four operons *mamAB*, *mms6*, *mamGFCD*, and *mamXY* (Fig. 1-2). The set of *mam* genes in the *mamAB* operon encoded essential and sufficient proteins for magnetosome formation (20, 21), while the *mms6*, *mamGFCD*, and *mamXY* operons encoded proteins have additive functions for synthesizing magnetite. The deletion of *mamAB* operon resulted to completely abolish the magnetic particles' formation. Besides, the AMB-1 mutant containing only *mamAB* operon, and lacking

mms6, *mamGFCD*, and *mamXY* operons, could synthesize the magnetic particles with severe defects in morphology and size of magnetite crystals (20, 21).

One of the most abundant proteins in magnetosome is MamA, which is encoded in *mamAB* operon. MamA is the first protein which is identified from the purified magnetosomes, and determined amino acid sequence in 1996 by Okuda et al. (22). MamA is conserved in the MAI of all known MTB (23). Recently, the detailed localization of MamA in the magnetosome structure has been studied. Even though MamA is a soluble cytoplasmic protein, previous studies using transmission electron microscopy (TEM) (24) and atomic force microscopy (AFM) (25) clearly demonstrated that MamA localizes in the magnetosome matrix, a proteinaceous layer surrounding magnetosome vesicles, of *Magnetospirillum* species (Fig. 1-3). That localization of MamA in magnetosome provides the knowledges to the function of MamA in magnetosome formation. Two different functions of MamA have been proposed independently based on two different approaches. One approach used a *mamA* deletion mutant in *M. magneticum* AMB-1, which showed no effect on membrane invagination or magnetosome chain alignment (26). These results, combined with the knowledge that most magnetosome vesicles are empty, suggested that MamA appears to function in activating or priming preformed magnetosomes for biomineralization (26). On the other hand, Yamamoto et al. used the AFM to observe chains of magnetosomes with and without MamA and proposed that MamA is anchored to the magnetosome membrane and may stabilize the magnetosome chain (25).

The primary structure of MamA consists of five tetratricopeptide repeat (TPR) motifs and one putative TPR motif (27) (Fig. 1-4A). TPR motif is well-known module which found in numerous proteins and served as mediators of protein-protein

interactions (28). A single TPR motif adopts a helix-turn-helix fold (Fig. 1-4B). Generally, TPR proteins contain multiple TPR motifs, which provide a super-helix structure to the protein structure. The super-helix structure yields a pair of concave and convex curved surfaces that function as binding sites for protein-protein interactions to form multiprotein complexes (Fig. 1-4C) (28, 29). Recently, the X-ray crystal structures of MamA from *M. magneticum* AMB-1 (30), *M. gryphiswaldense* MSR-1 (30), *Candidatus Magnetobacterium bavaricum* (31), and *Desulfovibrio magneticus* RS-1 (32) have been determined. The MamA's five TPR motifs packed into the super-helix structure (Fig. 1-4D). According to electrostatic potential calculation, MamA from *M. magneticum* AMB-1 showed the positive charged concave surface and the negative charged convex surface, which possibly mediate the protein-protein interaction (Fig. 1-4C) (30). In addition, Zeytuni et al. demonstrated that the N-terminal putative TPR motif functions in homo-oligomerization of MamA (30). The deletion of the putative TPR motif led to the disruption of MamA oligomer (~500-kDa) into the monomer (24-kDa). Taken these results together, Zeytuni et al. proposed that MamA contains at least three protein binding sites, a putative TPR binding site, a concave binding site, and a convex binding site (30). However, the identity of the protein that interacts with MamA remained undetermined. In this study, I study on the protein-protein interaction between MamA and other magnetosome-associated proteins.

The goal of this study is to identify the MamA binding partner in magnetosome. The soluble MamA proteins need to bind to other magnetosome proteins in order to anchor in magnetosomes (Fig. 1-5). The interaction between MamA and other magnetosome-associated proteins provide a clue to answer the question of how MamA binds to magnetosomes. Also, the insight into the detailed protein-protein interaction in

magnetosome can contribute to further understanding of the protein organization in the magnetosome, and can shed a light into understanding the functions magnetosome-associated proteins in the synthesis of magnetic organelles.

References

1. **Murat D, Byrne M, Komeili A.** 2010. Cell biology of prokaryotic organelles. *Cold Spring Harb. Perspect. Biol.* **2**:a000422.
2. **Kerfeld CA, Heinhorst S, Cannon GC.** 2010. Bacterial microcompartments. *Annu. Rev. Microbiol.* **64**:391-408.
3. **Cameron JC, Wilson SC, Bernstein SL, Kerfeld CA.** 2013. Biogenesis of bacterial organelle: The carboxysome assembly pathway. *Cell* **155**:1131-1140.
4. **Pfeifer F.** 2012. Distribution, formation, regulation of gas vesicles. *Nat. Rev. Microbiol.* **10**:705-715.
5. **Lindsay MR, Webb RI, Fuerst JA.** 1997. Pirellulosomes: a new type of membrane-bounded cell compartment in planctomycete bacteria of the genus *Pirellula*. *Microbiology* **143**:739-748.
6. **Yeates TO, Crowley CS, Tanaka S.** 2010. Bacterial compartment organelles: protein shell structure and evolution. *Annu. Rev. Biophys.* **39**:185-205.
7. **Kerfeld CA, Erbilgin O.** 2015. Bacterial microcompartments and the modular construction of microbial metabolism. *Trends Microbiol.* **23**:22-34.
8. **Chowdhury C, Sinha S, Chun S, Yeates TO, Bobik TA.** 2014. Diverse bacterial microcompartment organelles. *Microbiol. Mol. Biol. Rev.* **78**:438-468.
9. **Komeili A.** 2012. Molecular mechanisms of compartmentalization and biomineralization in magnetotactic bacteria. *FEMS Microbiol. Rev.* **36**:232-255.
10. **Faivre D, Schüler D.** 2008. Magnetotactic bacteria and magnetosomes. *Chem. Rev.* **108**:4875-4898.
11. **Bazylinski DA, Frankel RB.** 2004. Magnetosome formation in prokaryotes. *Nat.*

Rev. Microbiol. **2**:217-230.

12. **Lefèvre CT, Bazylinski DA.** 2013. Ecology, diversity, and evolution of magnetotactic bacteria. *Microbiol. Mol. Biol. Rev.* **77**:497-526.
13. **Komeili A.** 2007. Molecular mechanisms of magnetosome-formation. *Annu. Rev. Biochem.* **76**:351-366.
14. **Nies DH.** 2011. How iron is transported into magnetosomes. *Mol. Microbiol.* **82**:792-796.
15. **Fukuda Y, Okamura Y, Takeyama H, Matsunaga T.** 2006. Dynamic analysis of a genomic island in *Magnetospirillum* sp. strain AMB-1 reveals how magnetosome synthesis developed. *FEBS Letters* **3**:801-812.
16. **Grünberg K, Wawer C, Tebo BM, Schüler D.** 2001. A large gene cluster encoding several magnetosome proteins is conserved in different species of magnetotactic bacteria. *Appl. Environ. Microbiol.* **67**:4573-4582.
17. **Schübbe S, Kube M, Scheffel A, Wawer C, Heyen U, Meyerdierks A, Madkour MH, Mayer F, Reinhardt R, Schüler D.** 2003. Characterization of a spontaneous nonmagnetic mutant of *Magnetospirillum gryphiswaldense* reveals a large deletion comprising a putative magnetosome island. *J. Bacteriol.* **185**:5779-5790.
18. **Ullrich S, Kube M, Schübbe S, Reinhardt R, Schüler D.** 2005. A hypervariable 130-kilobase genomic region of *Magnetospirillum gryphiswaldense* comprises a magnetosome island which undergoes frequent rearrangements during stationary growth. *J. Bacteriol.* **187**:7176–7184.
19. **Lefèvre CT, Wu LF.** 2013. Evolution of the bacterial organelle responsible for magnetotaxis. *Trends Microbiol.* **21**:534-543.

20. **Murat D, Quinlan A, Vali H, Komeili A.** 2010. Comprehensive genetic dissection of the magnetosome gene island reveals the step-wise assembly of a prokaryotic organelle. *Proc. Natl. Acad. Sci. U.S.A.* **107**:5593-5598.
21. **Lohße A, Ulrich S, Katzmann E, Borg S, Wanner G, Richter M, Voigt B, Schweder T, Schüler D.** 2011. Functional analysis of the magnetosome island in *Magnetospirillum gryphiswaldense*: the *mamAB* operon is sufficient for magnetite biomineralization. *PLOS ONE* **6**:e25561.
22. **Okuda Y, Denda K, Fukumori Y.** 1996. Cloning and sequencing of a gene encoding a new member of the tetratricopeptide protein family from magnetosomes of *Magnetospirillum magnetotacticum*. *Gene* **171**:99-102.
23. **Lefèvre CT, Trubitsyn D, Abreu F, Kolinko S, de Almeida LGP, de Vasconcelos ATR, Lins U, Schüler D, Ginet N, Pignol D, Bazylinski DA.** 2013. Monophyletic origin of magnetotaxis and the first magnetosomes. *Environmental Microbiology* **15**:2267-2274.
24. **Taoka A, Asada R, Sasaki H, Anzawa K, Wu LF, Fukumori Y.** 2006. Spatial localizations of Mam22 and Mam12 in the magnetosomes of *Magnetospirillum magnetotacticum*. *J. Bacteriol.* **188**:3805-3812.
25. **Yamamoto D, Taoka A, Uchihashi T, Sasaki H, Watanabe H, Ando T, Fukumori Y.** 2010. Visualization and structural analysis of the bacterial magnetic organelle magnetosome using atomic force microscopy. *Proc. Natl. Acad. Sci. U.S.A.* **107**:9382-9387.
26. **Komeili A, Vali H, Beveridge TJ, Newman DK.** 2004. Magnetosome vesicles are present before magnetite formation, and MamA is required for their activation. *Proc. Natl. Acad. Sci. U.S.A.* **101**:3839-3844.

27. **Okuda Y, Fukumori Y.** 2001. Expression and characterization of a magnetosome-associated protein, TPR-containing MAM22, in *Escherichia coli*. FEBS Letters **491**:169-173.
28. **Zeytuni N, Zarivach R.** 2012. Structural and functional discussion of the tetra-trico-peptide repeat, a protein interaction module. Structure **20**:397-405.
29. **Kajander T, Cortajarena AL, Mochrie S, Regan L.** 2007. Structure and stability of designed TPR protein superhelices: unusual crystal packing and implications for natural TPR proteins. Acta. Cryst. D63:800-811.
30. **Zeytuni N, Ozyamak E, Ben-Harush K, Davidov G, Levin M, Gat Y, Moyal T, Brik A, Komeili A, Zarivach R.** 2011. Self-recognition mechanism of MamA, a magnetosome-associated TPR-containing protein, promotes complex assembly. Proc. Natl. Acad. Sci. U.S.A. **108**:E480-487.
31. **Zeytuni N, Baran D, Davidov G, Zarivach R.** 2012. Inter-phylum structural conservation of the magnetosome-associated TPR-containing protein, MamA. J. Struct. Biol. **180**:479-487.
32. **Zeytuni N, Cronin S, Lefèvre CT, Arnoux P, Baran D, Shtein Z, Davidov G, Zarivach R.** 2015. MamA as a model protein for structure-based insight into the evolutionary origins of magnetotactic bacteria. PLOS ONE. **10**(6):e0130394.

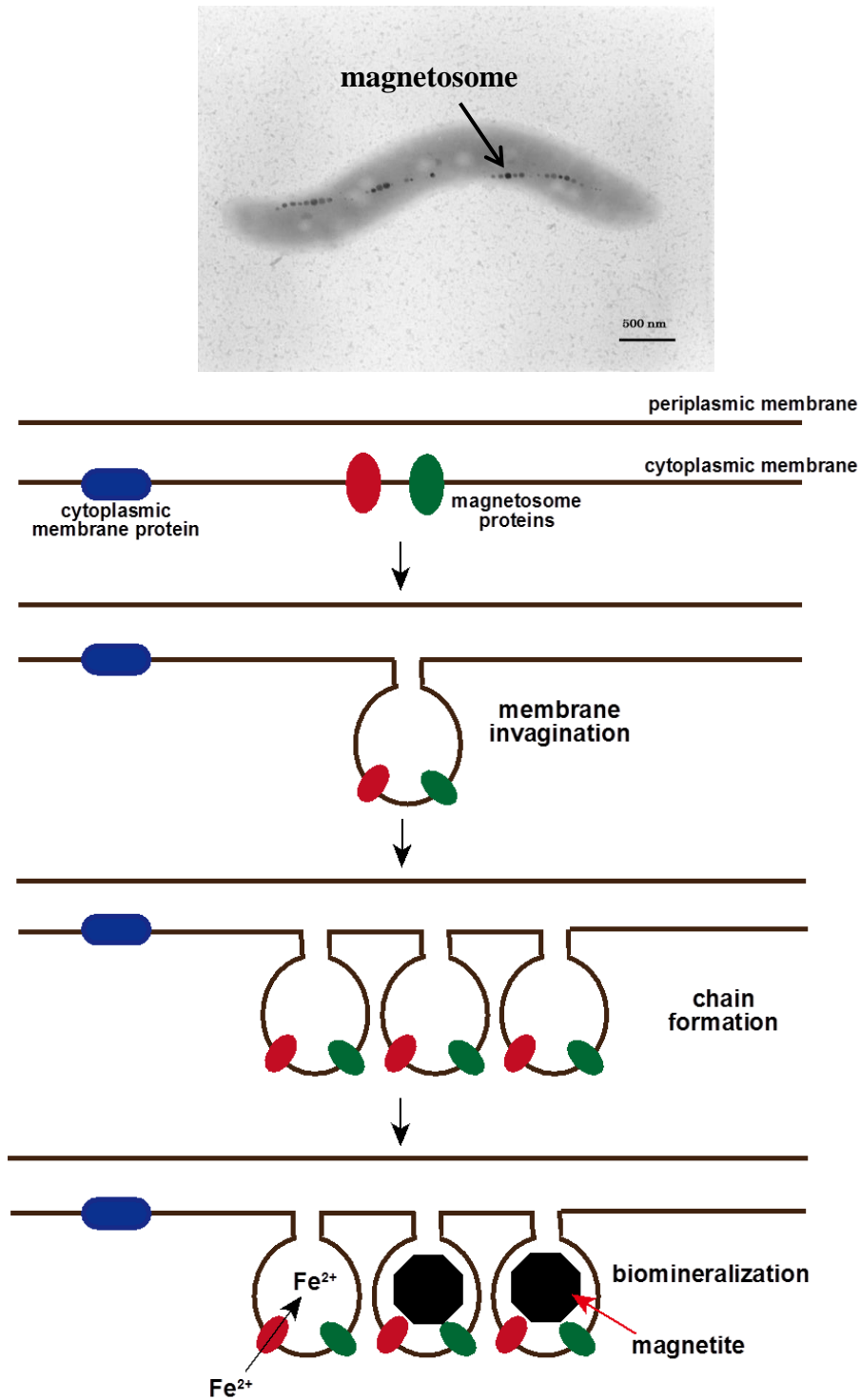


Figure 1-1. (Top) Transmission electron micrograph of *Magnetospirillum magneticum* AMB-1. (Bottom) Model for magnetosome formation. First, the magnetosome membrane is derived by the invagination of inner membrane. Second, individual vesicles are assembled into a chain. Third, iron ions are transferred into the magnetosome vesicles from cytoplasm using magnetosome specific iron transporters (14), then magnetite crystals are mineralized in the vesicles (modified the Komeili's model (13)).

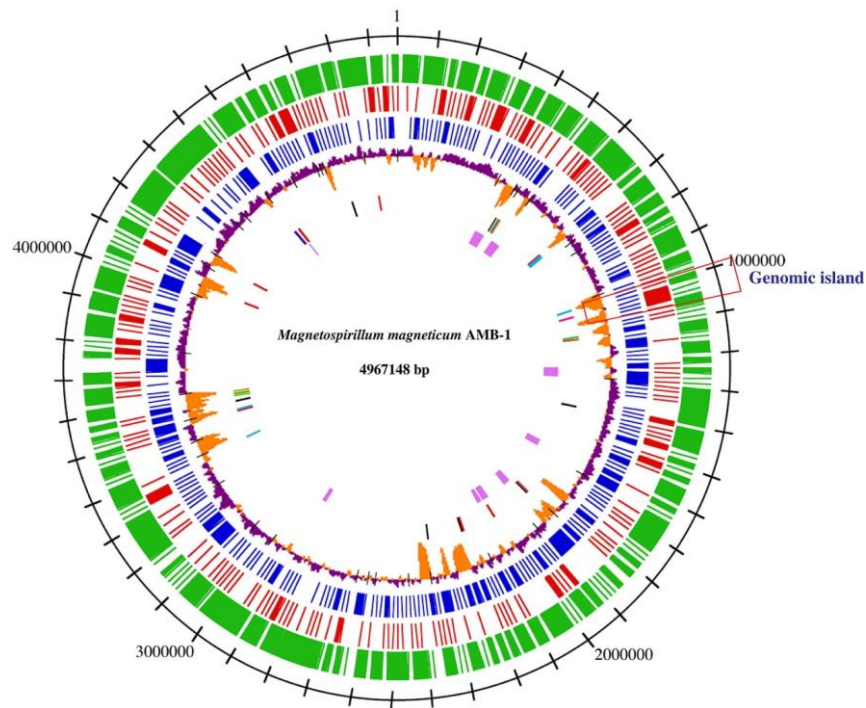
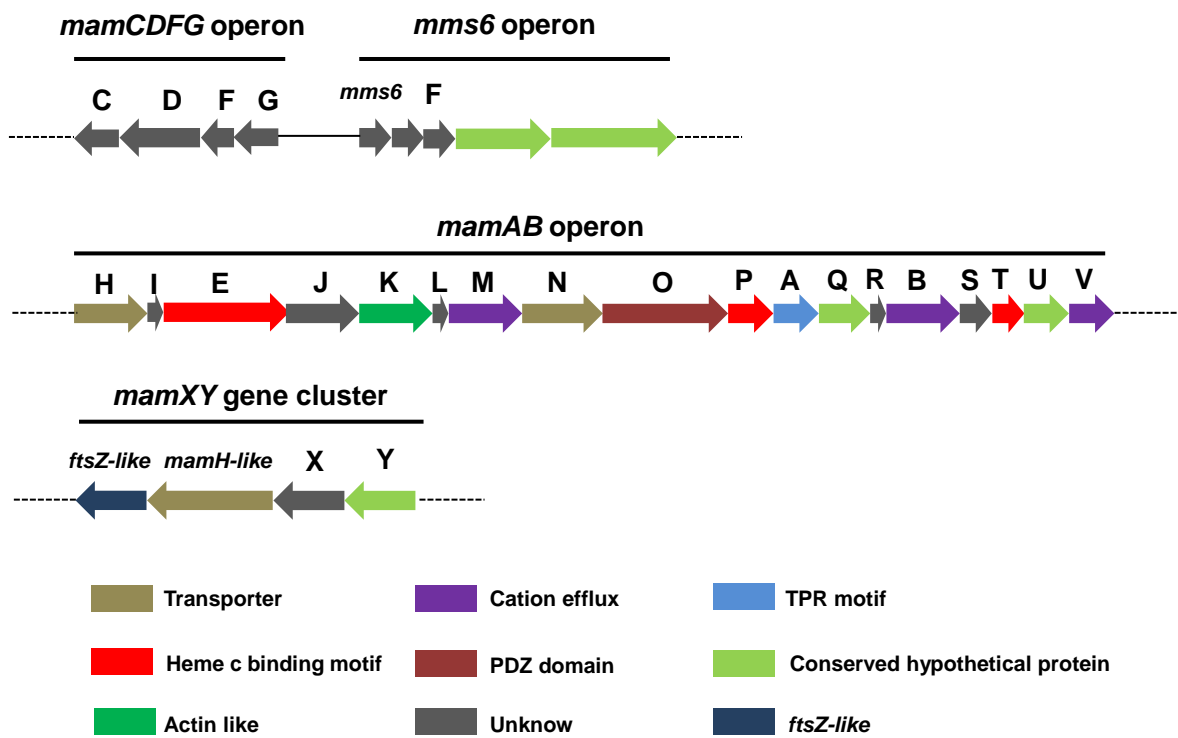
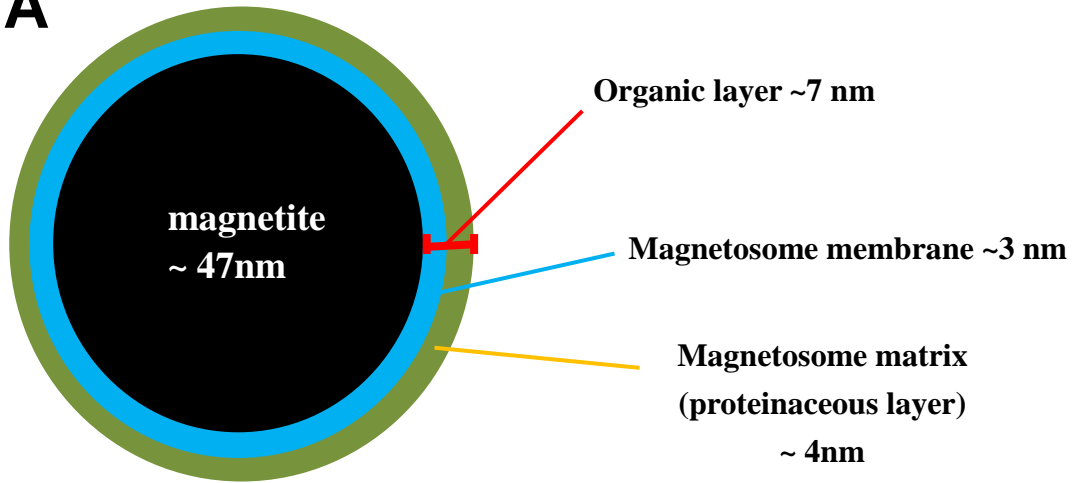
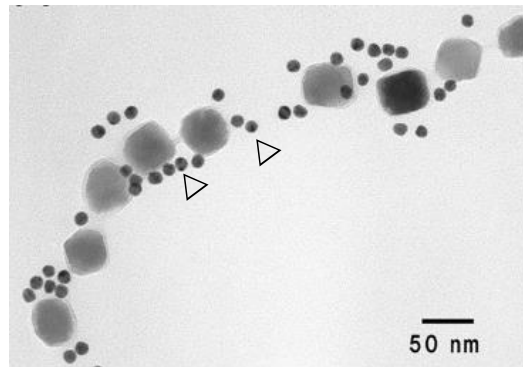
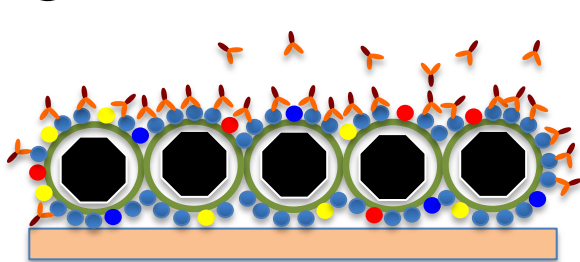
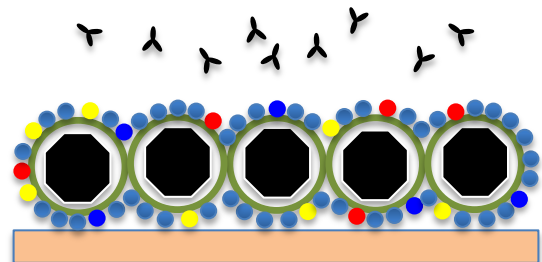
A**B**

Figure 1-2. (A) Circular representation of the 4967148-bp genome of *Magnetospirillum* sp. AMB-1 and other magnetic bacteria (Fukuda et al. (15)). The red box of genomic island indicates the 98-kb magnetosome island (994,000–1,099,000 bp in the AMB-1 genome). (B) Schematic view of magnetosome-associated proteins which are encoded within a magnetosome island of *M. magneticum* AMB-1. The genes encoding magnetosome associated proteins are involved in the four gene operons *mms6*, *mamGFDC*, *mamAB* and *mamXY*.

A**B****C**

Anti-MamA antibodies densely bound to the surface of the magnetosomes.



Pre-immune serum which has no significant affinity for MamA cannot bind to the surface of magnetosomes.

● : MamA
 ● ● ● : Other magnetosomal proteins

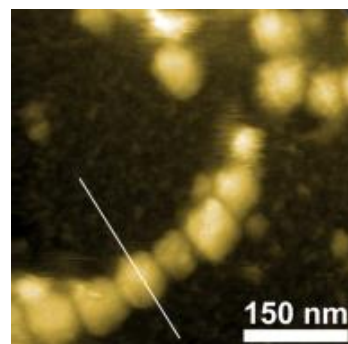
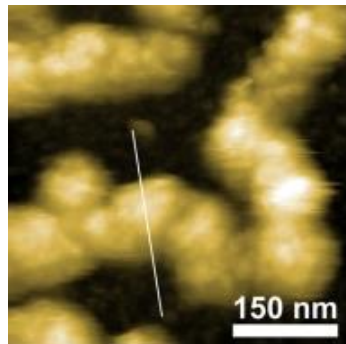
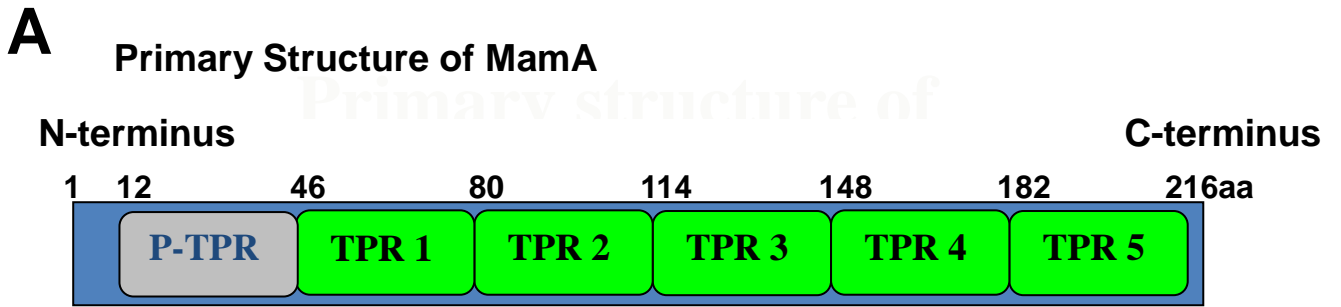


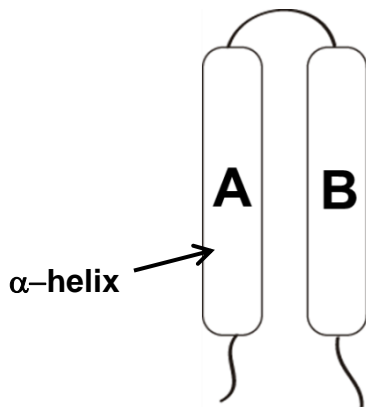
Figure 1-3. Spatial localization of MamA in the magnetosomes. (A) Schematic drawing of magnetosome. The individual magnetite crystal is surrounded by an organic layer (25). Magnetosomal matrix is a proteinaceous layer surrounding magnetosome vesicles. (B) Transmission electron micrograph of purified magnetosomes which were labelled with immunogold. Purified magnetosomes were incubated with polyclonal anti-MamA antibodies, followed by incubation with 15 nm gold-conjugated goat anti-rabbit IgG. Gold particles represented MamA (open arrowheads) localized on magnetosome matrix, indicating the localization of MamA (Taoka et al. (24)). (C) Atomic force micrographs of immune-labeled magnetosomes. (Top) Schematic drawing for the method of immuno-labelled magnetosomes. The purified magnetosome was incubated with polyclonal anti-MamA antibody or pre-immuno serum. (Bottom, left) MamA antibodies bound to magnetosomes. The dimension of magnetosomes increases in consistent with the diameter of antibody, indicating MamA located at the magnetosomes matrix. (Bottom, right) Pre-immuno serum which has no significant affinity for MamA cannot bind to the surface of magnetosomes (Yamamoto et al. (25)).



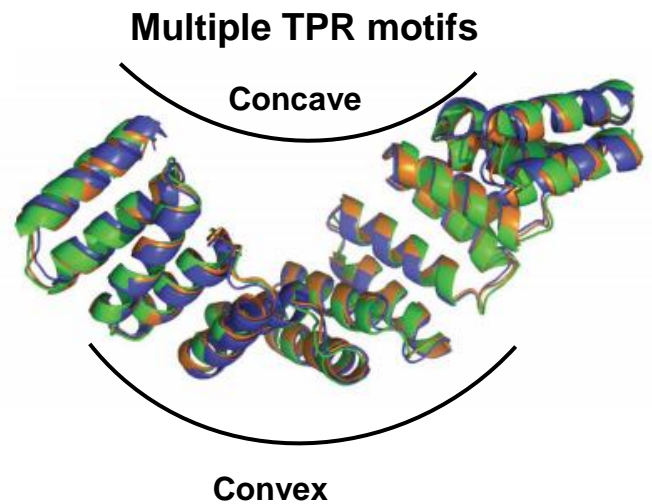
P-TPR: putative TPR

TPR: tetratricopeptide repeat motif

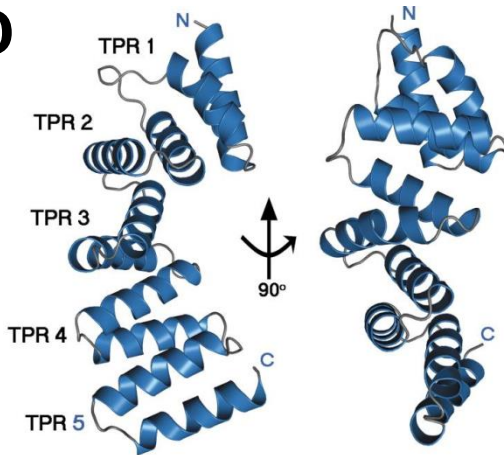
B Single TPR motif



C

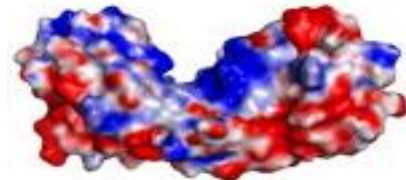


D



Putative binding sites of MamA:

Concave: positive charged



Convex: negative charged

Figure 1-4. (A) The primary structure of MamA. MamA consists of five TPR motifs and one putative TPR motif as previously described by Okuda et al. (27). (B) Schematic drawing of single TPR motif. The single TPR motif structure is helix-turn-helix. (C) Ribbon structure of multiple TPR motifs, e.g. 8 individual TPR motifs, show the concave and convex surfaces (29). (D) Ribbon structure of MamA Δ 41 (without the putative TPR) monomer showed that 5 TPR motifs of MamA yields concave and convex surfaces. According to electrostatic potential calculation, the concave surface is positive charged and the convex surface is negative charged as described by Zeytuni et al. (30, 31).

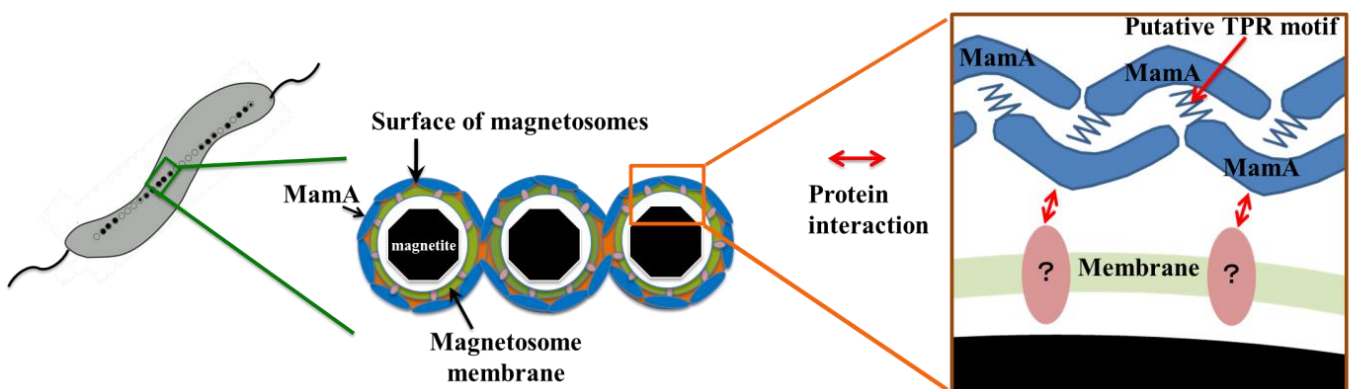


Figure 1-5. Model of the protein-protein interaction between MamA and other magnetosome associated proteins in magnetosomes. It has been proposed that MamA contains at least three protein binding sites, a putative TPR binding site, a concave binding site, and a convex binding site (30). The speculation is that the putative TPR motifs bind to the concave sites of other MamA monomers to form a homo-oligomer. The other site could bind other magnetosome-associated proteins because the soluble MamA proteins need to bind to other magnetosome proteins in order to anchor in magnetosomes. The goal of this study is to identify the MamA binding partners in magnetosomes.

Chapter II

**A protein-protein interaction in
magnetosome: TPR protein MamA
interacts with magnetite biomineralizing
protein Mms6**

Introduction

Even though MamA crystal structures have been determined, the function of protein-protein interaction of MamA still remains enigmatic. Previously, Taoka et al. reported that when the purified magnetosomes were treated with the alkaline buffer (CAPS-NaOH, pH 11.0), MamA was specifically removed from the magnetosomes, giving the MamA-eliminated magnetosomes (1). Interestingly, when the alkaline-treated magnetosomes were incubated with recombinant purified MamA, MamA localized around that magnetosomes. This result indicated that MamA binding partners exist in alkaline-treated magnetosomes and attached MamA.

According to this finding, Suzuki et al. has screened the MamA binding proteins from the protein extract of the MamA eliminated magnetosomes by the alkaline-treatments (2). First, Suzuki et al. prepared the MamA-affinity chromatography column by immobilizing the purified His-tag MamA to the CNBr-activated Sepharose resin (GE Healthcare). After, the extract of MamA-eliminated magnetosome proteins from *Magnetospirillum magneticum* AMB-1 was subjected to the column. The proteins absorbed on the column were eluted with the alkaline buffer. Finally, the eluted proteins were concentrated and identified by mass spectrometry. Figure 2-1 shows the list of the identified proteins. Five candidates of MamA binding proteins, methyl-accepting chemotaxis protein (amb1418), hypothetical protein (amb3421), porin (amb0025), ATP synthase epsilon chain (amb4138) and Mms6 (amb0956), were identified from *M. magneticum* AMB-1. Only Mms6 was the magnetosome-associated protein in the candidates of MamA binding proteins (Fig. 2-1).

My goal was to understand which magnetosome-associated protein binds to

MamA, therefore I focused on interaction between MamA and Mms6. Mms6, one of the well-studied magnetosome-associated proteins, is encoded in *mms6* operon which involved in biomineralizing magnetite crystals in *Magnetospirillum* species. Arakaki et al. identified Mms6 as a 6.0-kDa mature protein consisting of 59 amino acids, however the *mms6* gene sequence shows that the full-length of the Mms6 protein is 133 amino acids (3). The 6.0-kDa Mms6 protein is tightly bound to magnetite crystals and is involved in the biomineralization of cubo-octahedral magnetite crystals both *in vitro* (3, 4) and *in vivo* (5-7). An *mms6* deletion mutant was shown to synthesize smaller magnetite crystals with abnormal crystal morphologies, despite showing no effect on the structure of magnetosome vesicles (5, 6).

In this study, I proved the protein-protein interaction between two magnetosome constructing proteins, MamA and Mms6, by using immuno-precipitation, pull-down and size-exclusion chromatography experiments. In addition to this, I found that two different types of Mms6 exist in the magnetosome membrane, a 14.5-kDa and 6.0-kDa version. This study, for the first time, showed the presence of two types of Mms6 in the magnetosome. Also, the Mms6¹⁻¹³³ (14.5-kDa) was determined to interact with MamA.

Materials and Methods

Microorganisms and cultures.

Bacterial strains and plasmids are listed in Table 2-1. *M. magneticum* AMB-1 (ATCC 700264) was cultured in a modified magnetic spirillum growth medium (MSGS) (Table 2-2) under an O₂ (1%) – N₂ (99%) atmosphere at 28°C in the dark as previously described (8).

Escherichia coli strain XL-1 Blue MRF⁷ was cultivated in LB broth (9) at 37°C and was used for cloning study. Strain BL21(DE3) was cultivated at 30°C and used for protein expression. When necessary, the antibiotics kanamycin (20 µg/ml) or ampicillin (100 µg/ml) were added to the *E. coli* cultures.

Magnetosome purification.

Magnetosome purification was performed as previously described with some modifications (1). The frozen cells (20 g wet weight) were thawed out and suspended in 100 ml of 10 mM Tris-HCl buffer (pH 8.0). Cells then were disrupted by passing through a French press (1,000 kg f/cm²) three times and the pellet was collected by centrifuging at 8,000 × *g* for 15 min. The pellet was suspended in 10 mM Tris-HCl buffer (pH 8.0) and the suspension was placed on bar magnets for 5 h. The nonmagnetic fluid was removed by aspiration. The magnetosomes attracted to magnets were resuspended in 10 mM Tris-HCl buffer and this step was repeated at least 10 times. Finally, the purified magnetosomes were collected by centrifugation 8,000 × *g* for 15 min. The purified magnetosomes were suspended in 10 mM Tris-HCl buffer (pH 8.0) and stored at -80°C until used. All purification steps were carried out at 4°C.

Preparation of cellular components.

After disrupting AMB-1 cells as described above, the magnetosomes and cell debris were precipitated by centrifugation at $8,000 \times g$ for 15 min. The obtained supernatant was ultra-centrifuged at $100,000 \times g$ for 1 h and the supernatant and the pellet was used as the soluble fraction and the membrane fraction, respectively. Besides, magnetosomes were purified from the pellet as described above. For SDS-PAGE and immunoblot analyses, the proteins were extracted from the membrane fraction and the magnetosome fraction by incubation with 2% SDS at 37°C for 1 h.

Expression and purification of Mms6 proteins.

Primer sequences are shown in Table 2-3. For C-terminal His-tagged full-length Mms6 expression, the plasmid pET29b-mms6¹⁻¹³³ was constructed by cloning the entire PCR-amplified *mms6* gene (*mms6*¹⁻¹³³; accession number: AB096081) fragment into the *NdeI/KpnI* sites of pET-29b (Merck-Millipore). The plasmid pET29b-mms6¹⁻¹³³-a was constructed in this study using a primer set (FW-mms6-a and RV-mms6-a) to remove the linker sequence between thrombin site and His-tag (Fig. 2-2). The plasmid DNA fragment was amplified by PCR. The PCR product was ligated and transformed into *E. coli* XL-1 Blue MRF'. The recombinant plasmids obtained from *E. coli* XL-1 Blue MRF' were then sequenced (Eurofins Genomics). The pET29b-mms6¹⁻¹³³-a was also used as the template to create the pET29b-mms6⁷⁵⁻¹³³. The recombinant plasmid pET29b-mms6⁷⁵⁻¹³³ was ligated, transformed into *E. coli* XL-1 Blue MRF' and then was sequenced. After, pET29b-mms6⁷⁵⁻¹³³ was introduced into *E. coli* strain BL21(DE3) for the expression of Mms6⁷⁵⁻¹³³-His (Fig. 2-2).

For protein expression, *E. coli* strain BL21(DE3) containing these recombinant plasmids were grown at 30°C until an $A_{600\text{ nm}}$ of ~0.6, and then induced by 1 mM (final concentration) of isopropyl- β -D-thiogalactopyranoside (IPTG) for 7 h in a jar fermenter. The cells were then harvested by centrifuging at $8,000 \times g$ for 15 min.

To purify recombinant Mms6¹⁻¹³³-His (expressed by pET29b-mms6¹⁻¹³³) and Mms6⁷⁵⁻¹³³-His (expressed by pET-mms6⁷⁵⁻¹³³), cells (~ 6.0 g wet weight) were suspended in 10 mM Tris-HCl (pH 8.0) and disrupted using sonication (80 W for 15 min). The lysate was centrifuged at $8,000 \times g$ for 15 min to remove the cell debris, and then the supernatant was ultra-centrifuged at $100,000 \times g$ for 1 h to separate the membrane and the soluble fractions. The expressions of Mms6 proteins in membrane or soluble fractions were analyzed by SDS-PAGE (Fig. 2-3). Both of Mms6¹⁻¹³³ and Mms6⁷⁵⁻¹³³ were localized in the membrane fractions. In order to solubilize the Mms6 proteins, ten kinds of commercially available detergents were tested for solubilization of Mms6 from the membrane fraction (Fig. 2-4). In this study, the CHAPS was selected to solubilize Mms6 proteins due to the high solubility of Mms6 proteins.

For purification of Mms6 proteins, the membrane fraction was suspended in 10 mM Tris-HCl (pH 8.0) containing 2% CHAPS and 200 mM NaCl, and then incubated at 4°C for 2 h to solubilize the Mms6 proteins. The solubilized fraction was harvested by ultracentrifugation ($100,000 \times g$ for 1 h) and the supernatant was subjected to a Ni-NTA resin (QIAGEN) column equilibrated with 50 mM NaH₂PO₄ buffer (pH 8.0) containing 10 mM imidazole, 0.2% CHAPS and 300 mM NaCl. After the column was washed with 50 mM NaH₂PO₄ buffer (pH 8.0) containing 50 mM imidazole, 0.2% CHAPS and 300 mM NaCl, the proteins bound to the column were eluted with 50 mM NaH₂PO₄ buffer (pH 8.0) containing 250 mM imidazole, 0.2% CHAPS and 300 mM NaCl. The eluted

protein fraction was dialyzed against 10 mM Tris-HCl (pH 8.0) containing 0.2% CHAPS. The purified proteins were analyzed by SDS-PAGE (Fig. 2-5).

Purification of MamA

Unlike Mms6 protein, N-terminal His-tagged MamA was expressed in the soluble fraction (10). The soluble fraction, derived from ultra-centrifuging the cell-free extract, was subjected to a Ni-NTA resin (QIAGEN) column equilibrated with 50 mM NaH₂PO₄ buffer (pH 8.0) containing 10 mM imidazole and 300 mM NaCl. The column unbound proteins were washed with 50 mM NaH₂PO₄ buffer (pH 8.0) containing 50 mM imidazole, and 300 mM NaCl. The proteins absorbed to the column were eluted with 50 mM NaH₂PO₄ buffer (pH 8.0) containing 250 mM imidazole and 300 mM NaCl. The eluted MamA protein fraction was dialyzed against 10 mM Tris-HCl (pH 8.0) and used for protein-protein interaction experiments.

Physical and chemical measurements.

SDS-PAGE was performed using the method of Laemmli (11) and tricine-SDS-PAGE was performed as previous described (12) to separate the low molecular mass proteins. Comassive Brilliant Blue G-250 (Wako) was used as a gel-staining dye. The protein concentration was determined using a BCA Protein Assay Kit (Thermo Fisher Scientific). UV-VIS spectrophotometer (UV-2550, Shimadzu) was used to measure the absorbance of chemical substance to the light.

Immunoblotting analyses.

Anti-Mms6¹⁻¹³³ polyclonal rabbit antibodies were raised against the purified

recombinant Mms6¹⁻¹³³-His. Immunoreactivity of anti-Mms6¹⁻¹³³ and anti-MamA antibodies (10) was detected at dilutions of 1:50,000 for each. Goat anti-Rabbit IgG conjugated to horseradish peroxidase (GE Healthcare Bioscience) was diluted 1:10,000 using the Pierce Western Blotting Substrate Plus (Thermo Fisher Scientific). The chemifluorescence data were collected using a Luminescent Image Analyzer, LAS 3000 (Fujifilm) and the band intensities were quantified using Multi Gauge software v. 2.2 (Fujifilm). The protein weights of the 14.5-kDa Mms6 and 6.0-kDa Mms6 from the purified magnetosomes were calculated according to the relative intensities for equal weights of these two protein bands in the immunoblot. The relative intensities for the 14.5-kDa Mms6 (Mms6¹⁻¹³³) and 6.0-kDa Mms6 (Mms6⁷⁵⁻¹³³) protein bands were calculated from the immunoblotting profiles of the two purified proteins, 0.1 µg Mms6¹⁻¹³³-His and 0.9 µg Mms6⁷⁵⁻¹³³-His, against anti-Mms6¹⁻¹³³ polyclonal antibodies (Fig. 2-6).

Immunoprecipitation assay

The immunoprecipitation assay was performed as previous described (13) with some modification. A 200 µl mixture containing 2 µM His-MamA and 1 µM Mms6¹⁻¹³³-His was incubated at 28°C for 1 h. After incubation, 2 µl of anti-Mms6¹⁻¹³³-antibody, anti-MamA antibody or normal serum were added to the mixture and incubated for 1 h. A slurry of protein A-Sepharose resin (GE Healthcare Bioscience) was added, and the proteins that co-precipitated with the protein A-Sepharose resin were analyzed by SDS-PAGE.

Pull-down assay

Pull-down assay is similar to the immunoprecipitation assay, except that a ‘bait’ protein is used to precipitate the protein-protein interaction instead of an antibody. Prior to performing the pull-down assay, the N-terminal poly-His of MamA was removed by using the Biotinylated Thrombin Kit (Novagen) (Fig. 2-7A). The solution of the 4 μM Mms6¹⁻¹³³-His, was incubated with 3 μM MamA at 25°C for 1 h. Afterwards, 15 μl of Ni-NTA agarose resin (QIAGEN), which had been equilibrated with buffer (50 mM NaH₂PO₄ containing 10 mM imidazole and 300 mM NaCl [pH 8.0]) was added to the solution. The resin was then washed five times with 400 μl of the same buffer. The bound proteins were eluted with 15 μl of elution buffer (50 mM NaH₂PO₄ containing 250 mM imidazole, and 300 mM NaCl [pH 8.0]) and the eluted proteins were analyzed by SDS-PAGE. In addition to this, the His-tag removed Mms6¹⁻¹³³ (Fig. 2-7B) was mixed with His-MamA and was precipitated with Ni-NTA agarose resin and the protein-protein interaction was analyzed by SDS-PAGE.

Size-exclusion chromatography.

Chromatography was performed at 4°C in a high pressure liquid chromatography (HPLC) system (GE healthcare) using a Superose 6 Increase 10/300GL column equilibrated with 10 mM Tris-HCl (pH 8.0) containing 0.2% CHAPS and 200 mM NaCl with a flow rate of 0.4 ml/min. Each fraction was collected at 1.25 min (0.5ml/fraction). Three markers were used, 669-kDa thyroglobulin (bovine thyroid), 220-kDa β -amylase (*Ipomoea batatas*), and 29-kDa carbonic anhydrase (bovine erythrocytes). For protein-protein interaction, a sample containing two proteins His-MamA (91 μg) and Mms6¹⁻¹³³-His (116 μg) was incubated for 1 hour at room temperature. All samples were centrifuged at 20,000 $\times g$ for 10 min prior to being

injected into the column.

Results and Discussion

Expression and purification of full-length Mms6¹⁻¹³³ and truncated mutant Mms6⁷⁵⁻¹³³

The screening of MamA binding proteins by using the affinity chromatography showed that the 14.5-kDa Mms6 is one of the binding candidates (Fig. 2-1). Previous to this result, Mms6 protein is known as a 6.0-kDa peptide that is associated with magnetite crystals and controls the size and morphology of crystals (3-7). Arakaki et al. (3) identified Mms6 as a 6.0-kDa mature protein consisting of 59 amino acids (from a. a. 75 to 133), but the *mms6* gene sequence shows that the full-length Mms6 protein is 133 amino acids (deduced a 14.5-kDa peptide) (Fig. 2-2).

In this study, I prepared the purified Mms6¹⁻¹³³ (14.5-kDa version of Mms6) and Mms6⁷⁵⁻¹³³ (6.0-kDa version of Mms6) proteins, and anti-Mms6 polyclonal antibodies for research tools. The anti-Mms6 antibodies raised against the Mms6¹⁻¹³³ peptide. Also, in order to study *in vitro* the interactions between MamA and Mms6, the full-length Mms6¹⁻¹³³ and truncated protein Mms6⁷⁵⁻¹³³ have been used.

At first, to examine the expression of full-length Mms6¹⁻¹³³ and truncated Mms6⁷⁵⁻¹³³, proteins from soluble fraction and membrane fraction were analyzed. Both Mms6¹⁻¹³³ and Mms6⁷⁵⁻¹³³ contained putative transmembrane region from a. a. 89 to 111 according to transmembrane prediction tool (TMHMM) (Fig. 2-2), therefore, they could localize in the membrane. According to SDS-PAGE analysis of cellular fraction, Mms6¹⁻¹³³ and Mms6⁷⁵⁻¹³³ were expressed in membrane fractions (Fig. 2-3). To solubilize Mms6 proteins, ten kinds of commercially available detergents were tested to solubilize Mms6 proteins including ionic, non-ionic, and zwitterionic detergents (Fig. 2-4). In the SDS-PAGE analysis of solubilized samples, although ionic detergents, such

as SDS, can solubilize most of the transmembrane proteins, such strong detergents denature protein structures, preventing protein-protein interactions. Otherwise, CHAPS in solution containing 200 mM NaCl could extract many Mms6 proteins and could be used to examine the protein-protein interaction (Fig. 2-4). Therefore, CHAPS detergent was selected to solubilize recombinant Mms6 proteins entire of this study. As a result in Figure 2-5, solubilized Mms6 proteins, Mms6¹⁻¹³³ and Mms6⁷⁵⁻¹³³, were highly purified from the membrane using Ni-NTA affinity chromatography.

Presence of a 14.5-kDa Mms6 in magnetosomes.

According to the MamA affinity chromatography, the 14.5-kDa Mms6 have been found in the eluted fraction. I confirmed the presence of the 14.5-kDa version of Mms6 in magnetosomes. To do this, the generated anti-Mms6¹⁻¹³³ polyclonal antibodies were used for the immunoblotting analysis of AMB-1 cellular fractions. I confirmed that the anti-Mms6¹⁻¹³³ antibodies could recognize both recombinant protein bands of Mms6¹⁻¹³³ and Mms6⁷⁵⁻¹³³ (Fig. 2-6). I fractionated cellular proteins to the soluble proteins, the membrane proteins, and magnetosome proteins as described in Material and Methods. According to the immunoblotting analyses of the fractions, I found two positive bands that were specifically localized in the magnetosome fraction, one at 14.5-kDa and another at 6.0-kDa (Fig. 2-8A). As a control experiment, I performed the immunoblotting with an excess amount of Mms6¹⁻¹³³ (antigen), confirming that the cross-reactions of these two bands, 6.0-kDa and 14.5-kDa, were specific (Fig. 2-8A). Using immunoblotting, I quantified the ratio of 14.5-kDa and 6.0-kDa Mms6 bands in the magnetosome extracts using two different preparation methods. Method 1: incubating in 2% SDS at 37°C for 1 h, Method 2: incubating in boiling 1% SDS for 1.5

h and taking an aliquot every 30 min (the same method used by Arakaki et al. (3)) (Fig. 2-8B). In each method, both types of Mms6 were detected, but are present in different amounts. I calculated the ratio of 14.5-kDa and 6.0 kDa Mms6 protein amounts from the intensities of the protein bands in the immunoblots. The signal intensity for the Mms6¹⁻¹³³ band was 23 times stronger than that for the Mms6⁷⁵⁻¹³³ band for an equal weight of proteins (Fig. 2-6). The ratios were 63% and 37% for 14.5-kDa Mms6 and 6.0-kDa Mms6, respectively for method 1; and 38% and 62% for 14.5-kDa Mms6 and 6.0-kDa Mms6, respectively for method 2 (Fig. 2-8C). This result showed, for the first time, that two different sizes of peptides of Mms6 exist in the magnetosome, and they are present in different amounts depending on the method of preparation.

The interaction between MamA and 14.5-kDa Mms6.

I confirmed the protein-protein interaction between MamA and 14.5-kDa Mms6 (Mms6¹⁻¹³³) by immunoprecipitation and pull-down assay (Fig. 2-9). Immunoprecipitation was performed using His-tagged Mms6¹⁻¹³³ and His-tagged MamA, and two different antibodies, anti-MamA and anti-Mms6¹⁻¹³³, in different combinations to prove the binding between the two peptides (Fig. 2-9A). This demonstrated that Mms6¹⁻¹³³ co-precipitated with MamA (Fig. 2-9A). In the control experiment, there was no interaction (Fig. 2-9A). Additionally, the Ni-NTA pull-down assay designed to test the specific interaction between MamA and Mms6¹⁻¹³³ demonstrated that they did co-precipitate (Fig. 2-9B). I also confirmed the interaction between MamA and Mms6¹⁻¹³³ using size-exclusion chromatography (SEC). When I applied MamA and Mms6¹⁻¹³³ individually to SEC, MamA (Fig. 2-10) and Mms6¹⁻¹³³ (Fig. 2-11) were separately eluted in different fractions. MamA and Mms6¹⁻¹³³ formed

large oligomers with different molecular mass of ~500-kDa and >1,000-kDa, respectively. The results were consistent with previous studies which showed the oligomeric status of MamA and Mms6 (14, 15). Whereas, when I applied the mixture of MamA and Mms6¹⁻¹³³ to the column they were eluted in the same fractions at near the void volume of the column (Fig. 2-12), indicating that both proteins interacted. In this chapter, I determined the interaction between MamA and 14.5-kDa Mms6 by immunoprecipitation, pull-down, and size-exclusion chromatography.

This chapter clarifies the function of MamA in protein-protein interaction. Even though the results in this chapter clearly indicated that MamA interacts with Mms6, many questions remain to the detail of this protein-protein interaction. For example, which does Mms6's region involve in the binding to MamA? Does MamA bind to the 6.0-kDa Mms6 and is it the same binding site as the 14.5-kDa Mms6?

References

1. **A. Taoka, R. Asada, H. Sasaki, K. Anzawa, L.F. Wu, Y. Fukumori**, Spatial localizations of Mam22 and Mam12 in the magnetosomes of *Magnetospirillum magnetotacticum*, *J. Bacteriol.* 188 (2006) 3805-3812.
2. **E. Suzuki**. 磁性細菌の磁気オルガネラに局在する TPR 蛋白質に関する研究. Master dissertation (2012), Kanazawa University.
3. **A. Arakaki, J. Webb, T. Matsunaga**, A novel protein tightly bound to bacterial magnetic particles in *Magnetospirillum magneticum* strain AMB-1, *J. Biol. Chem.* 278 (2003) 8745-8750.
4. **Y. Amemiya, A. Arakaki, S.S. Staniland, T. Tanaka, T. Matsunaga**, Controlled formation of magnetite crystal by partial oxidation of ferrous hydroxide in the presence of recombinant magnetotactic bacterial protein Mms6, *Biomaterials* 28 (2007) 5381-5389.
5. **M. Tanaka, E. Mazuyama, A. Arakaki, T. Matsunaga**, MMS6 protein regulates crystal morphology during nano-sized magnetite biomineralization *in vivo*, *J. Biol. Chem.* 286 (2011) 6386-6392.
6. **A. Arakaki, A. Yamagishi, A. Fukuyo, M. Tanaka, T. Matsunaga**, Co-ordinated functions of Mms proteins define the surface structure of cubo-octahedral magnetite crystals in magnetotactic bacteria, *Mol. Microbiol.* 93 (2014) 554-567.
7. **D. Murat, V. Falahati, L. Bertinetti, R. Csencsits, A. Körnig, K. Downing, D. Faivre, A. Komeili**, The magnetosome membrane protein, MmsF, is a major regulator of magnetite biomineralization in *Magnetospirillum magneticum* AMB-1, *Mol. Microbiol.* 85 (2012) 684-699.

8. **R.P. Blakemore, D. Maratea, R.S. Wolfe**, Isolation and pure culture of a freshwater magnetic spirillum in chemically defined medium, *J. Bacteriol.* 140 (1979) 720-729.
9. **J.R. Sambrook, D.W. Russel**, *Molecular Cloning: A Laboratory Manual*, third ed., Cold Spring Harbor Laboratory, 2001.
10. **Y. Okuda, Y. Fukumori**, Expression and characterization of a magnetosome-associated protein, TPR-containing MAM22, in *Escherichia coli*, *FEBS Letters* 491 (2001) 169-173.
11. **U.K. Laemmli**, Cleavage of structural proteins during assembly of the head of bacteriophage T4, *Nature* 227 (1970) 680-685.
12. **H. Schägger**, Tricine-SDS-PAGE, *Nature Protocols* 1 (2006) 16-22.
13. **E.A. Golemis, P.D. Adams**, *Protein-Protein Interaction*, Cold Spring Harbor Laboratory Press, Cold Spring Harbor, New York, 2005, pp. 55-65.
14. **D. Yamamoto, A. Taoka, T. Uchihashi, H. Sasaki, H. Watanabe, T. Ando, Y. Fukumori**, Visualization and structural analysis of the bacterial magnetic organelle magnetosome using atomic force microscopy, *Proc. Natl. Acad. Sci. U.S.A.* 107 (2010) 9382-9387
15. **L. Wang, T. Prozorov, P.E. Palo, X. Liu, D. Vaknin, R. Prozorov, S. Mallapragada, M. Nilsen-Hamilton**, Self-assembly and biphasic iron-binding characteristics of Mms6, a bacterial protein that promotes the formation of superparamagnetic magnetite nanoparticles of uniform size and shape, *Biomacromolecules* 13 (2012) 98-105.

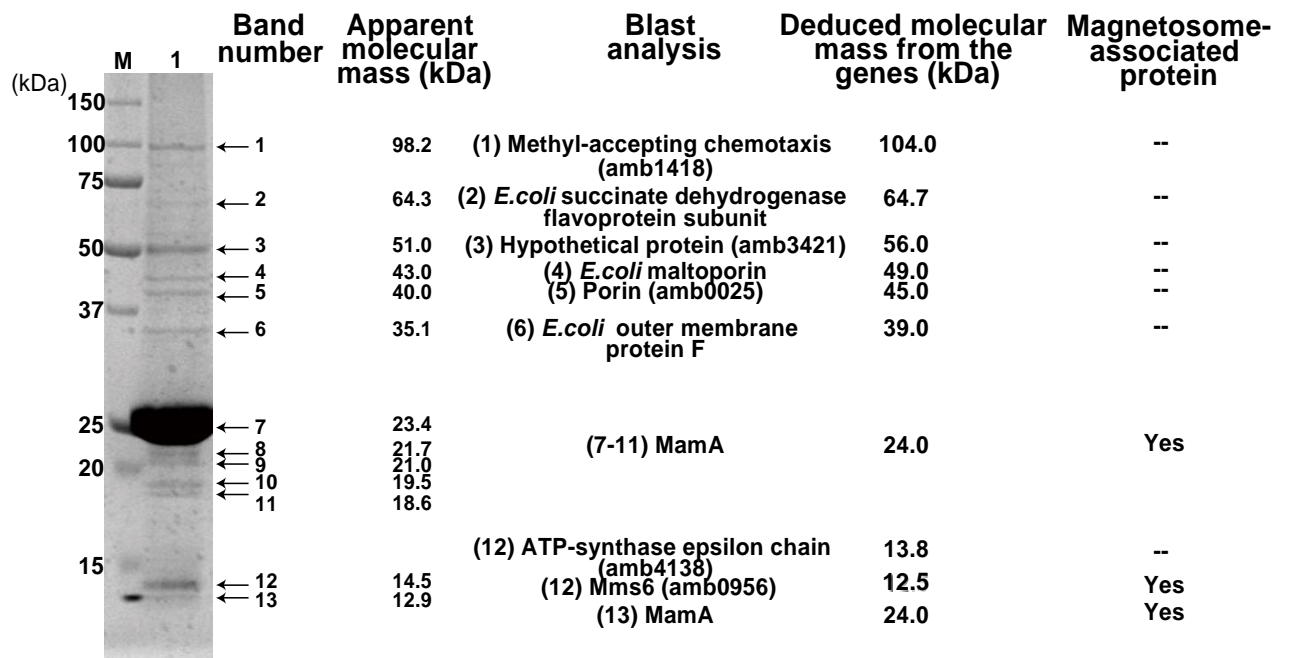


Figure 2-1. SDS-PAGE gel profile of proteins eluted from the His-MamA column and their apparent molecular masses (2). Protein extract from MamA-eliminated magnetosomes was applied to the column and the proteins binding to column were eluted by alkaline buffer; lane M, protein markers (Precision Plus protein standards; Bio-Rad); lane 1, eluted proteins. The eluted fractions were concentrated approximately 200 times for SDS-PAGE. These 13 bands were analyzed using tandem mass spectrometry and identified. Bands 2, 4, and 6 were proteins belonging to *E. coli*; bands 1, 3, 5, and 12 were proteins belonging to *M. magneticum* AMB-1; and bands 7-11, and 13 were recombinant MamA proteins. Only two of the bands were identified as magnetosome associated proteins, Mms6 and MamA. The gel was stained with Coomassie Brilliant Blue G-250.

A

Amino acids sequence of Mms6:

```

1 MGEMEREGAA AKAGAAKTGA AKTGTVAKTG IAAKTGVATA 40
41 VAAPAAPANV AAAQGAGTKV ALGAGKAAAG AKVVGTTIWT 80
81 GKGLGLGLGL GLGAWGPIIL GVVGAGAVYA YMKSRDIESA 120
121 QSDDEEVELRD ALA 133
  
```

B

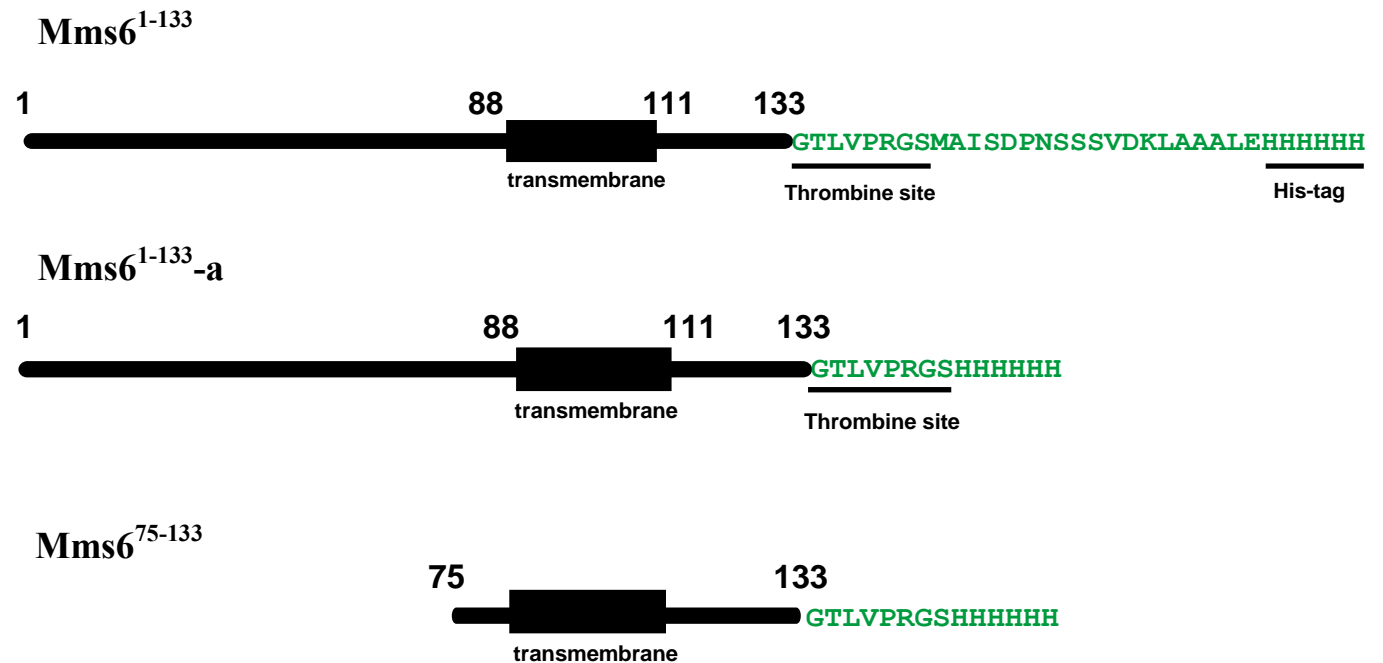


Figure 2-2. (A) The primary sequence of full length Mms6. Transmembrane region is showed in bold. Transmembrane region has been predicted using TMHMM (<http://www.cbs.dtu.dk/services/TMHMM/>). The arrowhead marked the 6-kDa Mms6 polypeptide. (B) Schematic drawing of primary structures of recombinant Mms6 proteins used in this chapter. Mms6¹⁻¹³³ is the 14.5-kDa peptide, and Mms6⁷⁵⁻¹³³ is the 6.0-kDa peptide.

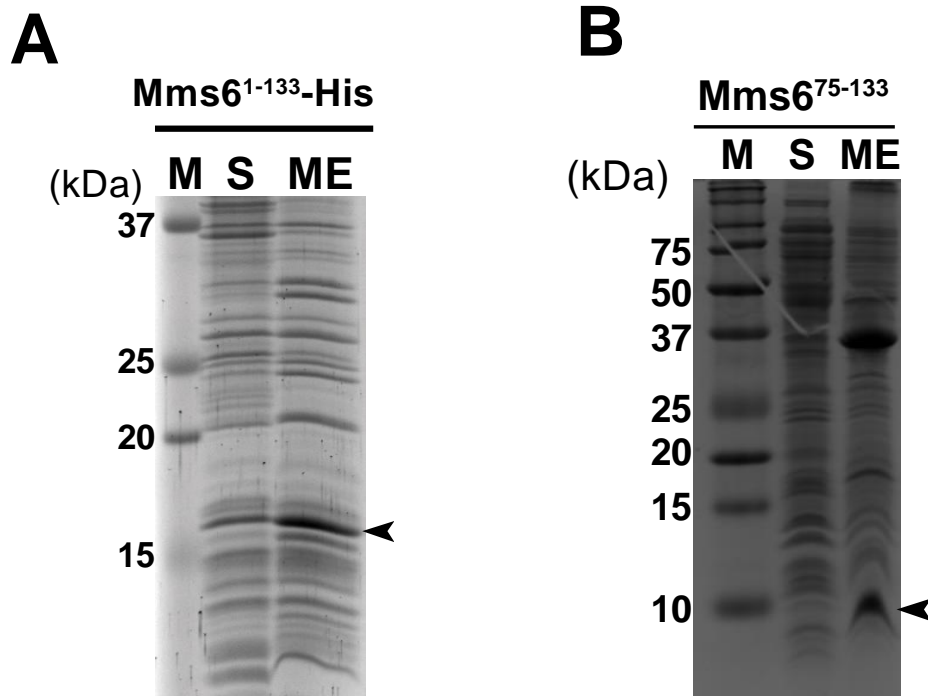


Figure 2-3. Analyses of Mms6 proteins' expressions. (A) SDS-PAGE gel profiles of Mms6¹⁻¹³³-His and (B) Tricine-SDS-PAGE gel profiles of Mms6⁷⁵⁻¹³³-His. Lane M is protein markers (Precision Plus protein standards; Bio-Rad); lane S is soluble fraction; lane ME is membrane fraction. For SDS-PAGE analyses, the proteins were extracted from the membrane fraction by incubation with 2% SDS at 37°C for 1 h. Both Mms6¹⁻¹³³-His and Mms6⁷⁵⁻¹³³-His were expressed in the membrane fractions. The arrowheads indicated recombinant proteins. The gels were stained with Coomassie Brilliant Blue G-250.

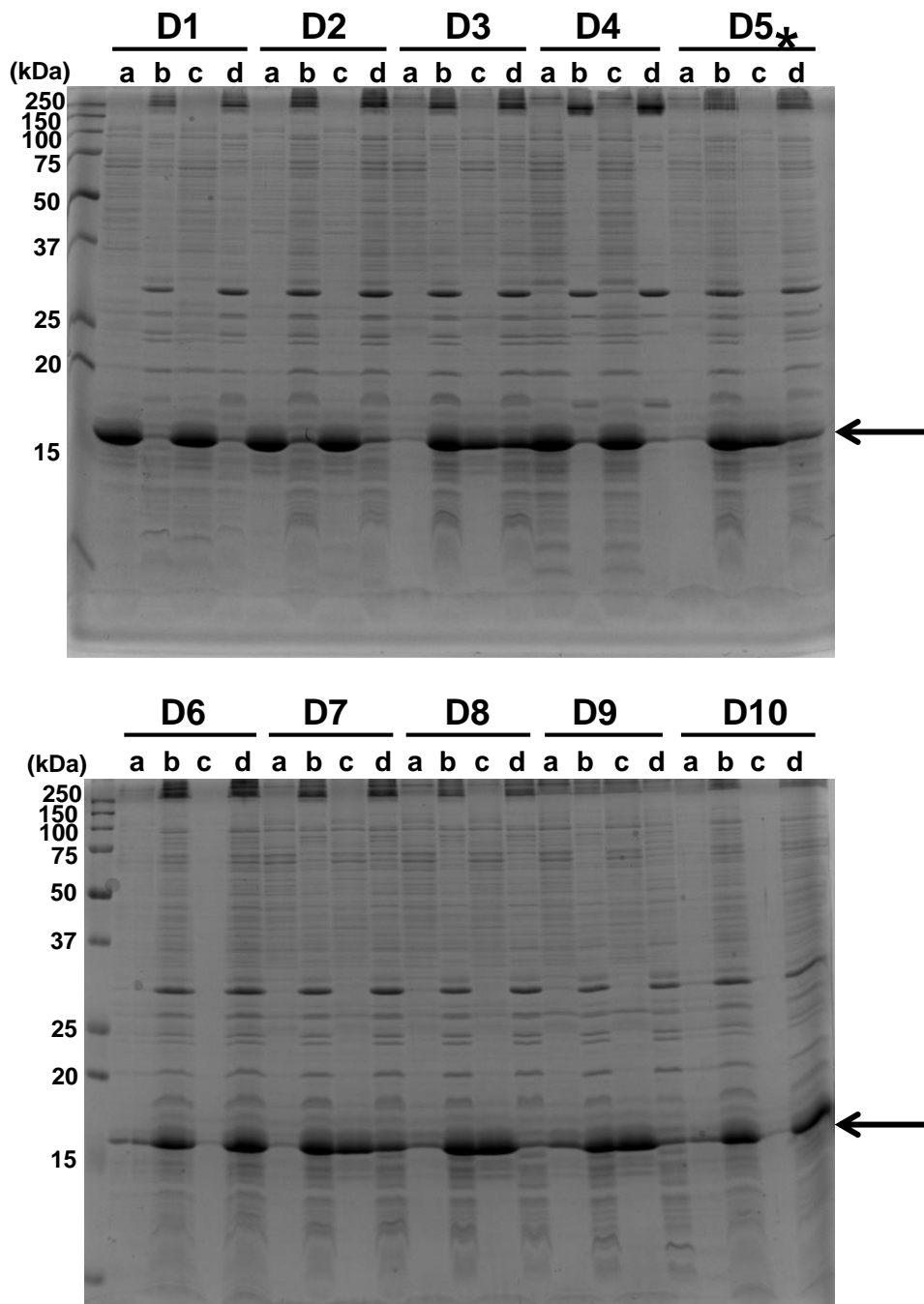


Figure 2-4. SDS-PAGE gel profiles of solubilized Mms6 from *E. coli* membrane fractions by ten kinds of detergents as follows:

D1: Sodium Deoxycholate

D6: MEGA 10

a: solubilized fraction

D2: Sodium Cholate

D7: Triton X-100

b: insolubilized fraction

D3: Nodide P40

D8: Sucrose monocaprato

c: solubilized frac. (200mM NaCl)

D4: N-laurylsarcosin

D9: n-Octyl- β -D-glucose

d: insolubilized frac. (200mM NaCl)

D5: **CHAPS**

D10: n-Octyl- β -D-thioglucose

The arrows indicate the Mms6¹⁻¹³³ protein bands.

* Note that the detergent **CHAPS (D5)** containing 200 mM NaCl was used to solubilized membrane proteins in this study.

Purified proteins

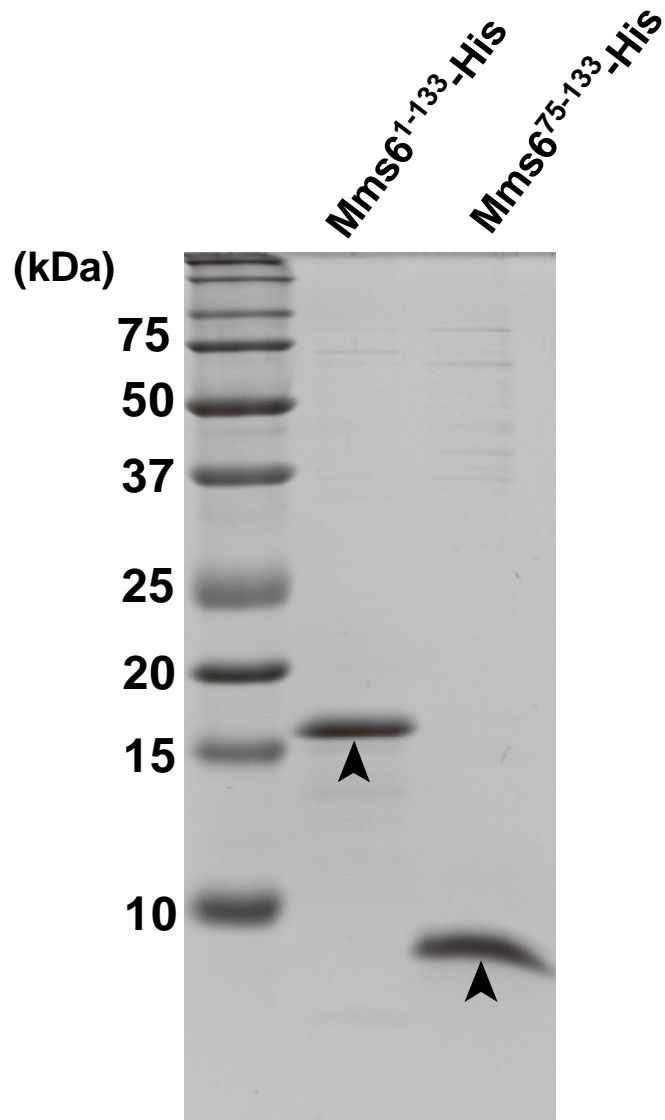


Figure 2-5. Purification of Mms6 proteins using Ni^{2+} affinity chromatography. Tricine-SDS-PAGE gel profile of purified Mms6 proteins. The solubilized Mms6 proteins, *Mms6*¹⁻¹³³ and *Mms6*⁷⁵⁻¹³³, were purified from the membrane fractions. The arrowheads indicated purified Mms6 proteins. The gels were stained with Coomassie Brilliant Blue G-250.

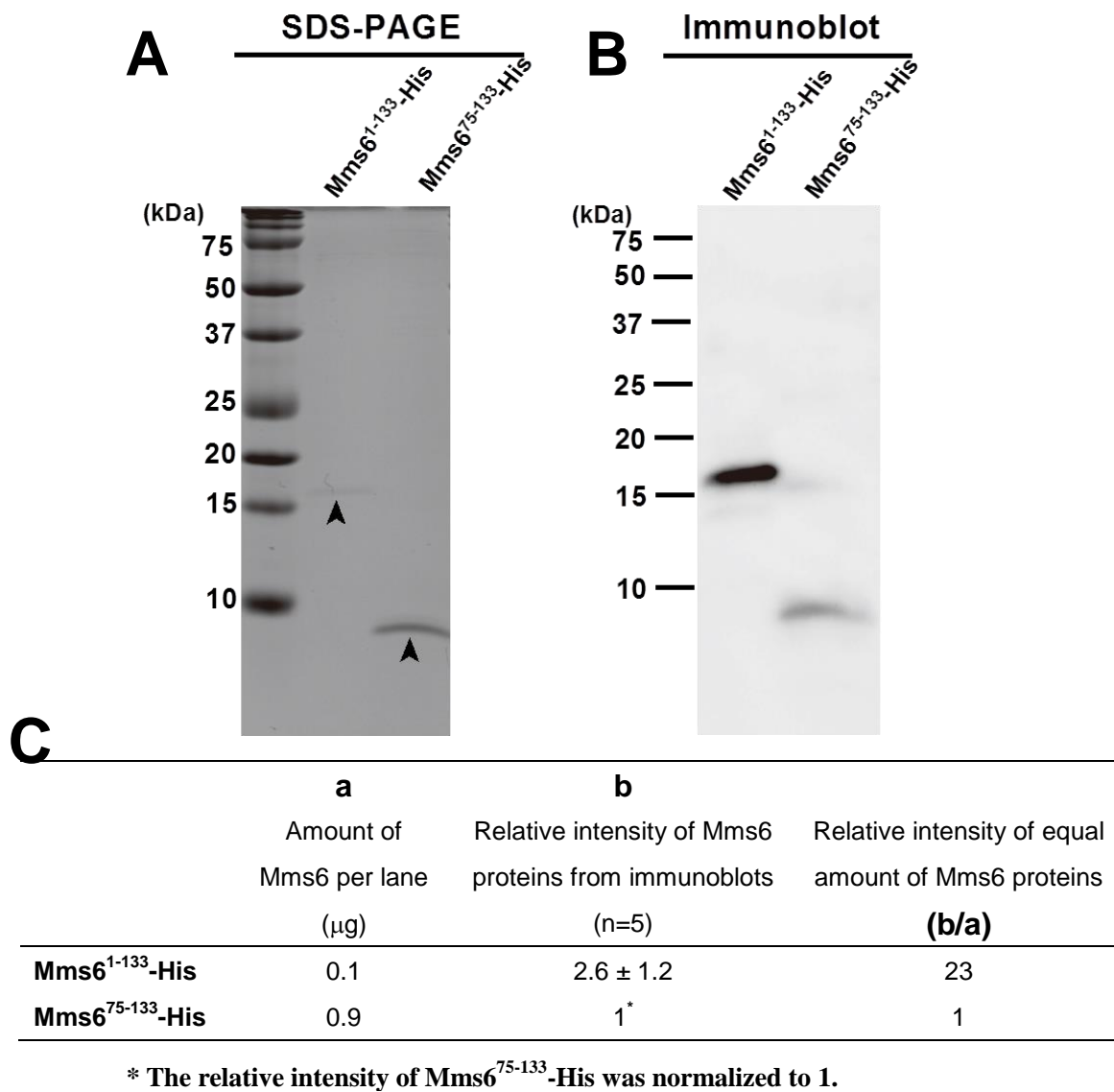


Figure 2-6. (A) The two different recombinant Mms6 peptides, Mms6¹⁻¹³³-His (0.1 μg) and Mms6⁷⁵⁻¹³³-His (0.9 μg) were definitively resolved on the gel (arrowheads). (B) The immunoblot of the samples in panel A using anti-Mms6¹⁻¹³³ antibodies. The five independent immunoblots were used to determine the relative intensity of two different peptides. (C) Table showing the relative intensity between the full length Mms6 peptide Mms6¹⁻¹³³-His and the shorter Mms6⁷⁵⁻¹³³-His. The relative intensity was determined from Multi Gauge software v. 2.2 (Fujifilm) and the shorter peptide was normalized to 1. The relative intensity was divided by the amount of protein used and the longer peptide, Mms6¹⁻¹³³-His, was found to be present 23X more relative to the shorter peptide, Mms6⁷⁵⁻¹³³-His. The gels were tricine gels stained with Coomassie Brilliant Blue G-250 and the marker is indicated on the left side of the gels (Precision Plus protein standards; Bio-Rad).

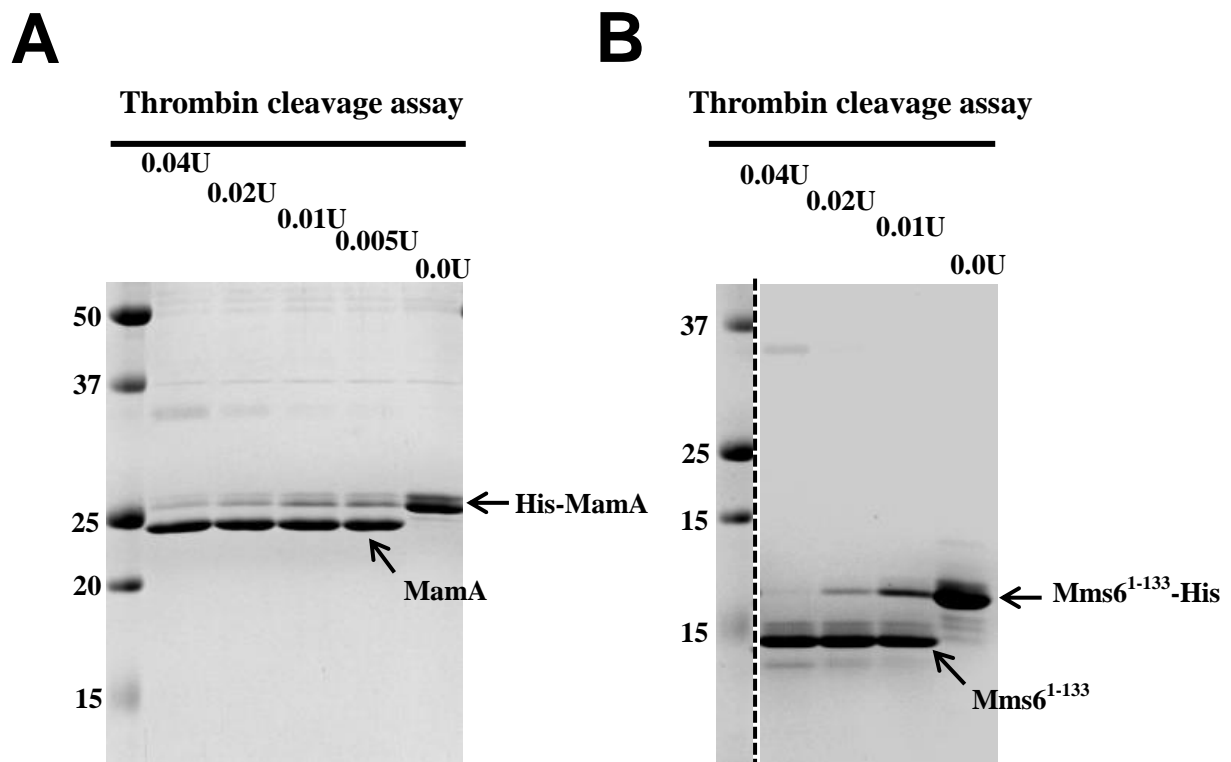


Figure 2-7. SDS-PAGE gel profiles of thrombin cleavage assays. (A) The N-terminal poly-His of MamA was removed by the reaction with different concentrations of Biotinylated Thrombin (U/ μ l) (Novagen) for 16 h at 4°C. (B) The C-terminal poly-His of Mms6¹⁻¹³³ was removed by the reaction with different concentrations of Biotinylated Thrombin (U/ μ l) (Novagen) for 16 h at room temperature. Reaction mixtures were removed the Biotinylated Thrombin by using Streptavidin Agarose. The His-tag removed proteins obtained were used for pull-down assay. Gels were stained with Coomassie Brilliant Blue G-250.

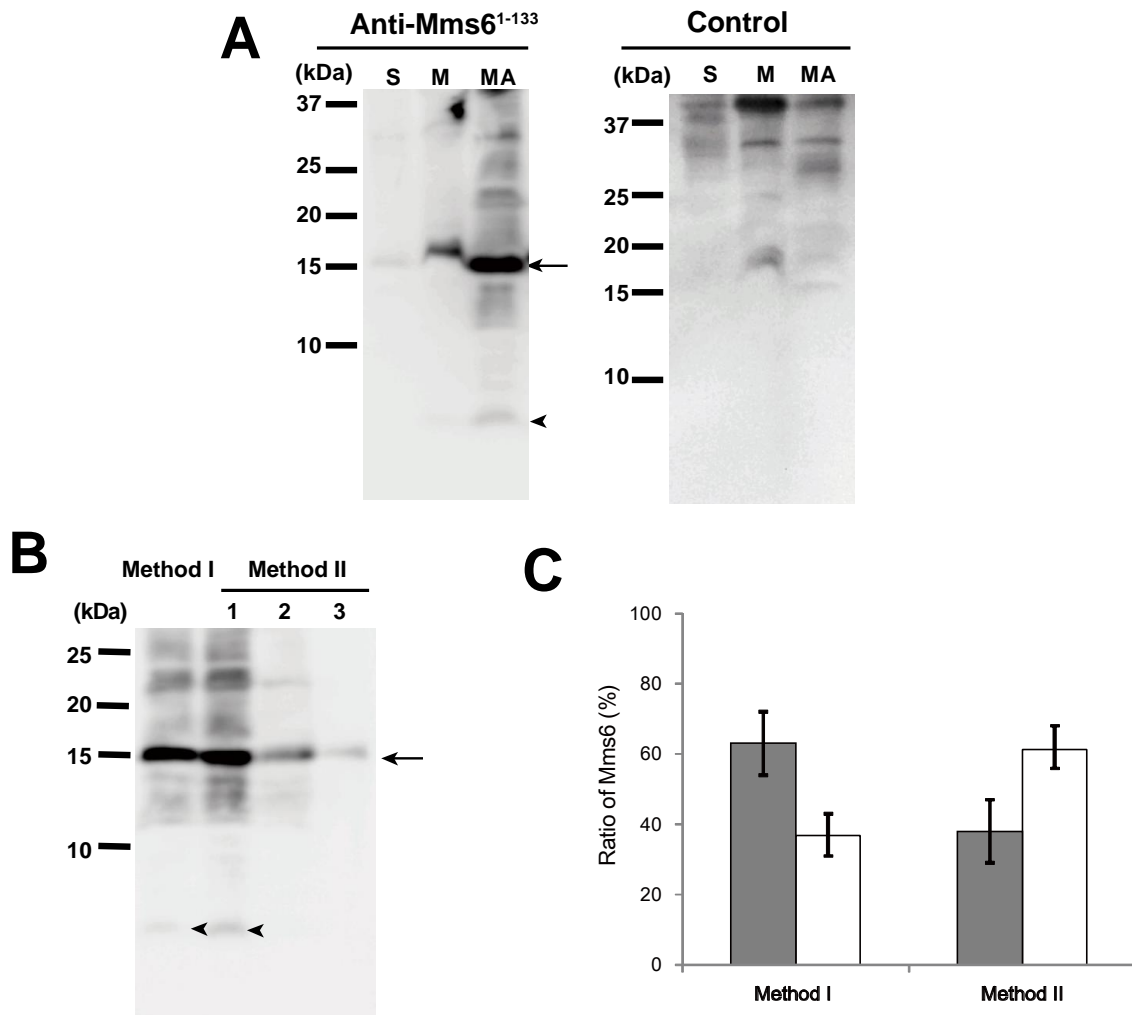


Figure 2-8. (A) Immunoblotting of *M. magneticum* AMB-1 extracts labeled with anti-Mms6¹⁻¹³³ polyclonal antibodies [left]. Two different Mms6 bands are evident, one at 14.5-kDa (arrow) and the other at 6.0-kDa (arrowhead). In the control experiment, the immunoblotting was carried out with an excess amount of Mms6¹⁻¹³³ antigen. In the control, the 14.5-kDa and 6.0-kDa bands were not detected [right]. S: soluble fraction; M: membrane fraction; MA: magnetosome fraction. (B) Two methods were used to extract Mms6 from the magnetosomes and then analyzed using immunoblotting. Method I used 2% SDS at 37°C for 1 h to extract. Method II was performed by Arakaki et al. (3) which extracted Mms6 by boiling magnetosomes in 1% SDS for 1.5 h with three aliquots taken every 30 min as lane 1, 2, and 3. Both two methods detected two types of Mms6 proteins. (C) Graph indicates the ratio of Mms6 protein amounts represented in magnetosomes according two methods of protein extraction. Different Mms6 proteins' ratios were calculated from the intensities of the protein bands 14.5-kDa and 6.0-kDa from three independent blots. The grey bars indicate 14.5-kDa Mms6 and the open bars indicate 6.0-kDa Mms6. The error bars represent the standard deviations.

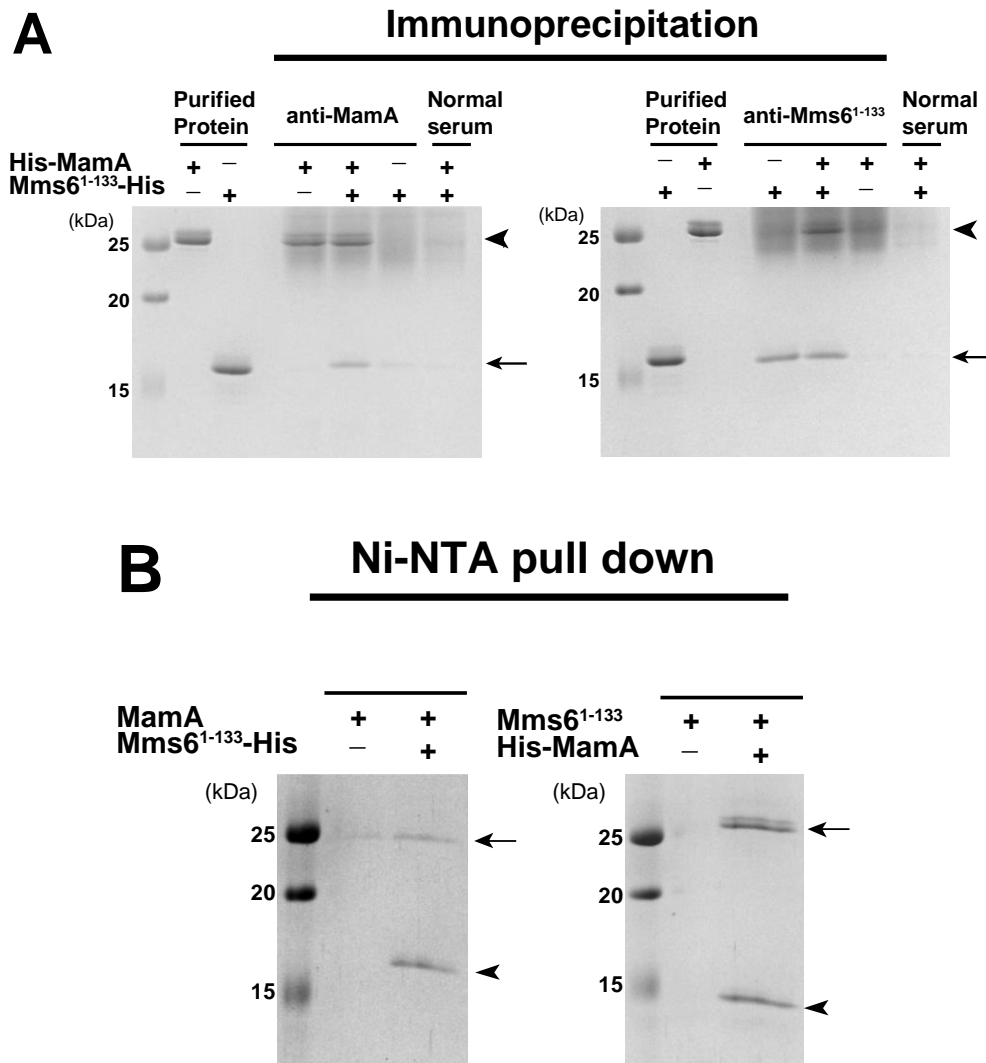


Figure 2-9. (A) SDS-PAGE analyses of the immunoprecipitation assays. A mixture containing His-MamA and Mms6¹⁻¹³³-His was precipitated with anti-MamA (left) or anti-Mms6¹⁻¹³³ (right) antibodies and clearly show that Mms6 (arrow) co-precipitates with MamA (arrowhead). When normal serum was used, there was no band for either MamA or Mms6 (right lanes). (B) SDS-PAGE analyses of the Ni-NTA agarose pull-down assay. The arrows indicated the His-MamA and the His-tag removed MamA protein bands; the arrowheads indicated the Mms6¹⁻¹³³-His and His-tag removed Mms6¹⁻¹³³ protein bands. Both the immunoprecipitation and pull-down assays confirm the interaction between MamA and Mms6¹⁻¹³³. The molecular mass standards (Precision Plus protein standards; Bio-Rad) are indicated on the left side of the gels. The gels were stained with Coomassie Brilliant Blue G-250.

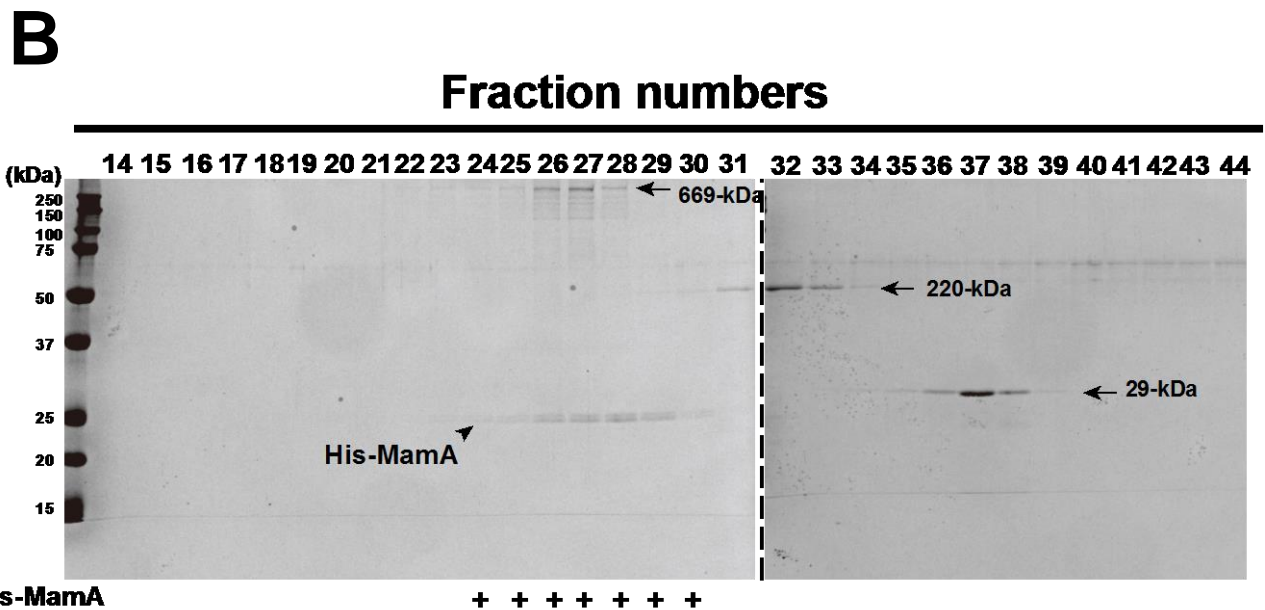
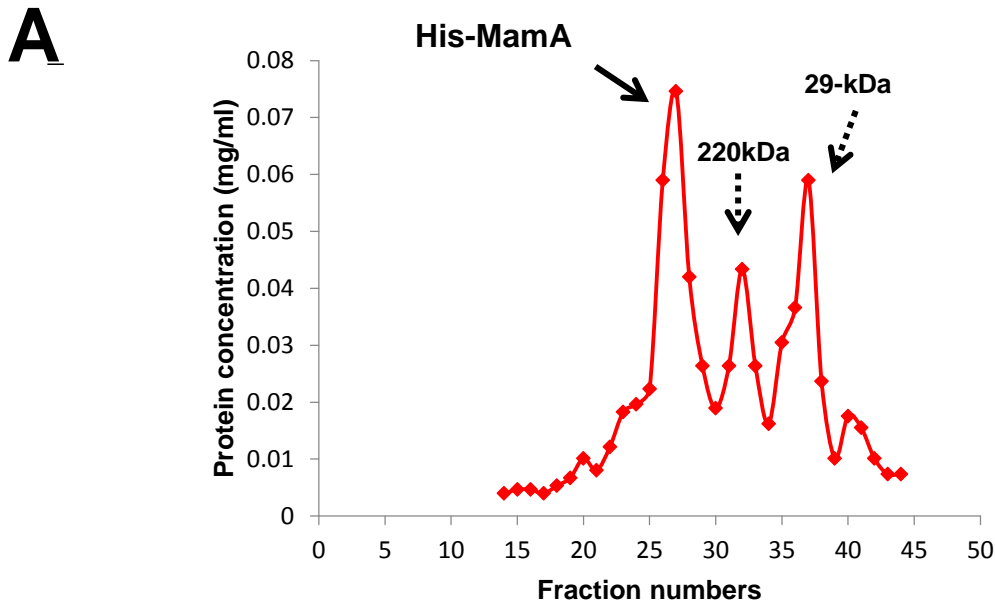


Figure 2-10. (A) Elution profile and (B) SDS-PAGE gel profile of His-MamA sample from size exclusion chromatography. MamA was eluted with molecular mass ~500.0-kDa, indicating that MamA forms oligomer. The bottom parts in SDS-PAGE profiles indicated the presence of proteins in eluted fractions. Three markers were used, 669-kDa thyroglobulin (bovine thyroid), 220-kDa β -amylase (*Ipomoea batatas*), and 29-kDa carbonic anhydrase (bovine erythrocytes).

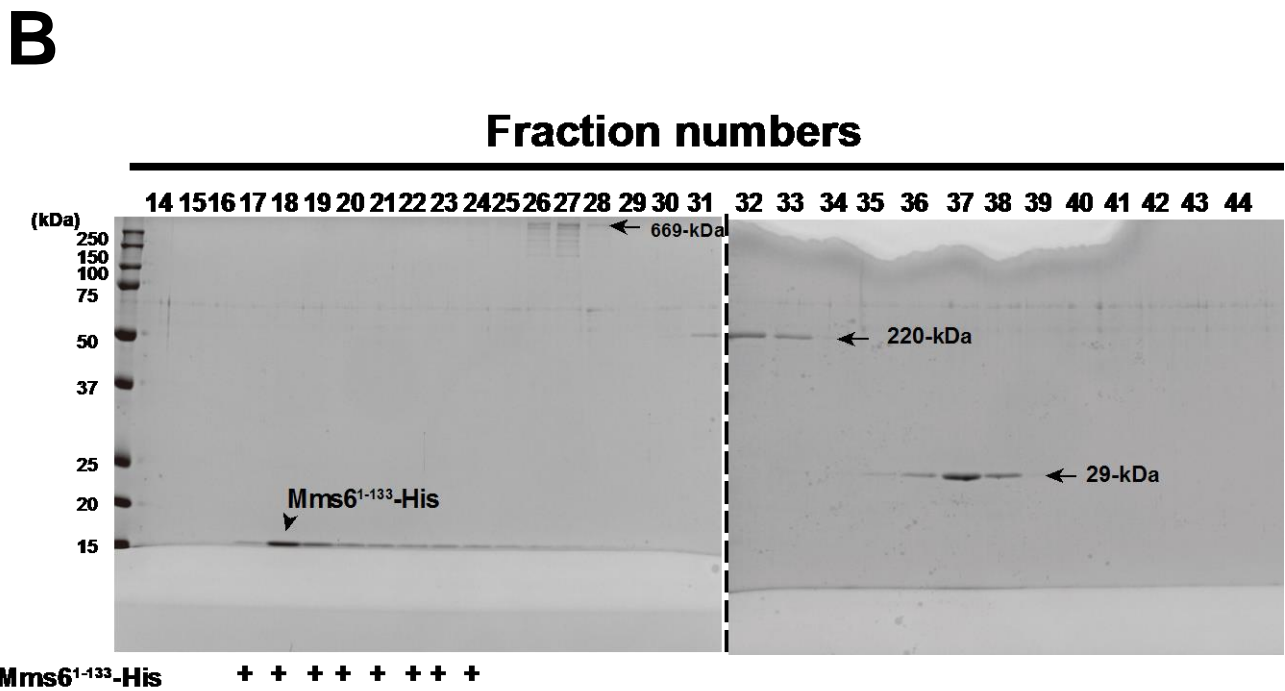
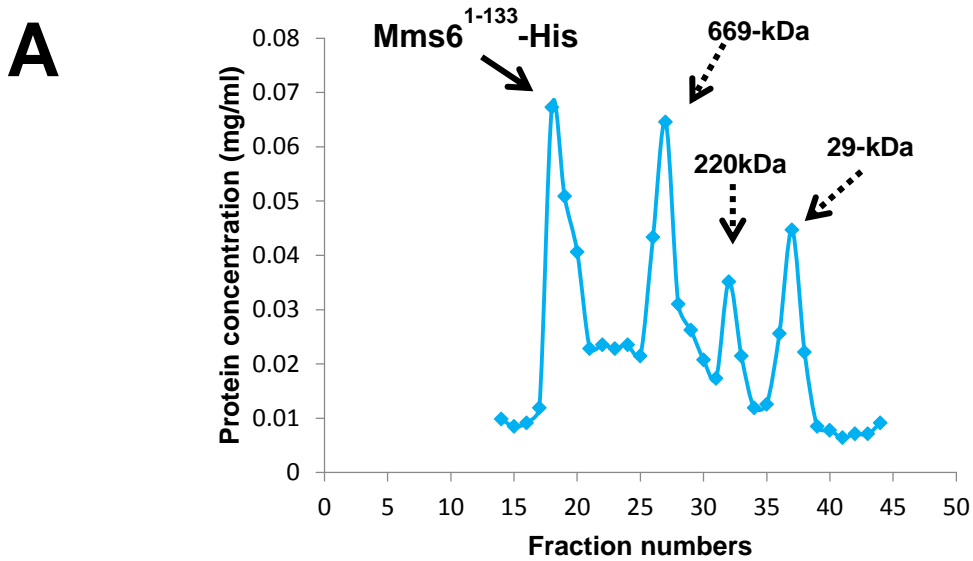


Figure 2-11. (A) Elution profile and (B) SDS-PAGE gel profile of Mms6¹⁻¹³³-His sample from size exclusion chromatography. Mms6¹⁻¹³³ forms larger oligomer with molecular mass >1,000-kDa. The bottom parts in SDS-PAGE profiles indicated the presence of proteins in eluted fractions. Three markers were used, 669-kDa thyroglobulin (bovine thyroid), 220-kDa β -amylase (*Ipomoea batatas*), and 29-kDa carbonic anhydrase (bovine erythrocytes).

Table 2-1. Bacterial strains and plasmids used in this study

Strains and plasmids	Description	Source or reference
<i>Strains</i>		
<i>M. magneticum</i> AMB-1		ATCC700264
<i>E. coli</i> XL-1 blue MRF ⁺	$\Delta(mcrA)183 \Delta(mcrCB-hsdSMR-mrr)173$ <i>endA1 supE44 thi-1 recA1 gryA96 relA1 lac</i> [F ⁺ , <i>proAB</i> , <i>laqI</i> ^{qZ} Δ M15, Tn10(Tet ^R)]	Stratagene
<i>E. coli</i> BL21(DE3)	<i>hsdS gal</i> (λ CIts857 <i>ind1 Sam7 nin5 lacUV5-T7</i> <i>gen I</i>)	Novagen
<i>Plasmids</i>		
pET-29b	Kan ^R , His (C-term), S-tag (N-term)	Novagen
pET15b-mamA	pET15b carrying <i>mamA</i> gene from AMB-1	(10)
pET29b-mms6 ¹⁻¹³³	pET29b carrying <i>mms6</i> ¹⁻¹³³ gene from AMB-1	Minamide (unpublished data)
pET29b-mms6 ¹⁻¹³³ -a	pET29b carrying <i>mms6</i> ¹⁻¹³³ gene from AMB-1	This study
pET29b-mms6 ⁷⁵⁻¹³³	pET29b carrying <i>mms6</i> ⁷⁵⁻¹³³ gene from AMB-1	This study

Table 2-2. Composition of chemically defined medium (MSGM) for cultivation of *Magnetospirillum magneticum* AMB-1

MSGM

Distilled water	1L
Wolfe's Vitamin Solution (see below)	10.0 ml
Wolfe's Mineral Solution (see below)	5.0 ml
Ferric Quinate Solution (see below)	2.0 ml
0.135% Resazurin	0.34 ml
KH ₂ PO ₄	0.68 g
NaNO ₃	0.12g
Ascorbic acid	0.035 g
Tartaric acid	0.37 g
Succinic acid	0.37 g
Sodium acetate	0.082 g

The pH of medium was adjusted to be 6.75 using NaOH

Wolfe's Vitamin Solution

Biotin	2.0 mg
Folic acid	2.0 mg
Pyridoxin HCl	10.0 g
Thiamine HCl	5.0 mg
Riboflavin	5.0 mg
Calcium D-(+)-pantothenate	5.0 mg
Nicotinic acid	5.0 mg
Cyanocobalamin	0.1 mg
p-Aminobenzoic acid	5.0 mg
Thioctic acid	5.0 mg
Distilled water	1 L

Wolfe's Mineral Solution

Nitrilotriacetic acid	1.5 g
MgSO ₄ 7H ₂ O	3.0 g
MnSO ₄ H ₂ O	0.5 g
NaCl	1.0 g
FeSO ₄ 7H ₂ O	0.1 g

CoCl ₂ 6 H ₂ O	0.1 g
CaCl ₂	0.1 g
ZnSO ₄ 7H ₂ O	0.1 g
CuSO ₄ 5H ₂ O	0.01 g
AlK(SO ₄) ₂ 12H ₂ O	0.01 g
H ₃ BO ₃	0.01g
Na ₂ MoO ₄ 2H ₂ O	0.01 g
Na ₂ SiO ₃	4.88 mg
Distilled water	1 L

Add nitrilotriacetic acid was dissolved in approximately 50 ml of water and pH was adjusted to be 6.5 with KOH to dissolve the compound.

Ferric Quinate Solution

FeCl ₃	0.27 g
Quinic acid	0.19 g
Distilled water	100 ml

Table 2-3. Primers used in this study.

Primer name	Sequence (5'-3')
FW -mms6-a	5'-CACCACCACCACCACCACTGAG-3'
RV -mms6-a	5'-GGAACCGCGTGGCACCAGGGTACC-3'
FW-mms6 75-133	5'-GGTGAACCATCTGGACCGG-3'
RV-mms6 75-133	5'-CATATGTATATCTCCTTCTTAAAG-3'

Chapter III

Identification of the MamA binding site in Mms6

Introduction

The study on protein-protein interactions is becoming important to understand the molecular mechanism of complex biological processes (1). Related to magnetosome formation, magnetosome-associated proteins have been intensely studied to determine how they synthesize magnetic particles; however, the functions of many magnetosome-associated proteins remain unclear. Protein-protein interaction plays a key role in predicting the function of magnetosome associated proteins during the creating, maintaining, and positioning the magnetosome organelles. For example, MamK and MamJ, two magnetosome-associated proteins encoded in *mamAB* operon, were detected to interact together by two-hybrid system analyses (2-4). MamK, a cytoskeleton structure protein, mediated the chain formation of magnetosomes (5, 6). The chain alignment of magnetosomes in cell from pole to pole works as a compass needle to orient MTB along the geomagnetic field. Besides, MamJ, a magnetosome membrane protein, was shown to associate with the filamentous structure of magnetosome and the deletion of MamJ results in the scattering of magnetosomes in cytoplasm (7). That MamK-MamJ interaction is essential to maintain the chain assembly of magnetosome, which creates a large magnetic moment passively aligned to a geomagnetic field.

In the chapter II, the protein-protein interaction of one well-known protein, TPR containing MamA, has been studied *in vitro* and I identified, for the first time, the MamA partner protein, Mms6, in magnetosome. Prior to this study, Mms6 was assumed to be only involved in magnetite biomineralization, however, my results suggested that Mms6 has an additional responsibility, binding to MamA. Besides, the result showed that two types of Mms6, 14.5-kDa and 6.0-kDa peptides, associated with magnetosomes.

A question remains as to the interaction between MamA and the 6.0-kDa short version of Mms6 (Mms6⁷⁵⁻¹³³). Therefore, it is necessary to examine the MamA-Mms6⁷⁵⁻¹³³ interaction and identify the MamA binding site in Mms6. The detailed protein-protein interaction between MamA and Mms6 will shed a light into understanding the function of these two magnetosome constructing proteins and the protein organization in magnetosomes.

In this chapter, I performed the mutational dissection of Mms6 to identify the protein-protein interaction between truncated mutant Mms6 and MamA. Using size-exclusion chromatography, immunoprecipitation and pull-down experiments, I obtained the results that the transmembrane region of Mms6 play a role in self-interaction to form the large oligomer and the oligomerization of Mms6 is necessary to the interaction with MamA oligomer.

Materials and Methods

Microorganisms and cultures.

Bacterial strains and plasmids are listed in Table 3-1. *Escherichia coli* strains XL-1 Blue MRF⁷ was used for cloning study and BL21(DE3) was used for protein expression. Prior to *E. coli* injection, the antibiotics kanamycin (20 µg/ml) was added to the medium.

Expression and purification of Mms6 proteins.

Primer sequences are shown in Table 3-2. The pET29b-mms6¹⁻¹³³-a was used as the template to create the expression plasmid of Mms6¹⁻¹¹¹-His and Mms6¹⁻⁸⁸-His (Fig. 3-1) with similar process described in Chapter II. For protein expression, *E. coli* strain BL21(DE3) containing these recombinant plasmids were grown at 30°C until an A_{600 nm} of ~0.6, and then induced by 1 mM (final concentration) of isopropyl-β-D-thiogalactopyranoside (IPTG) for 7 hours. The cells were then harvested by centrifuging at 8,000 × g for 15 minutes. Proteins expressed in *E. coli* were analyzed by SDS-PAGE of cellular fractions.

The recombinant Mms6¹⁻¹¹¹-His was purified as similar way to the purification of Mms6¹⁻¹³³ as described in chapter II. Mms6¹⁻⁸⁸-His was expressed in the soluble fraction (Fig. 3-2). Therefore, when the soluble protein fraction is derived after ultra-centrifuging the cell-free extract, the soluble proteins was subjected to a Ni-NTA resin (QIAGEN) column. The proteins bound to the column were eluted with 50 mM NaH₂PO₄ buffer (pH 8.0) containing 250 mM imidazole and 300 mM NaCl. The eluted protein fraction was dialyzed against 10 mM Tris-HCl (pH 8.0) containing 0.2% CHAPS and 200mM NaCl and used for protein-protein interaction experiments.

Physical and chemical measurements.

All of chemical and physical measurements in used in this study were similar to that described in previous chapter. In addition, His-tagged protein bands were visualized using InVision His-Tag In-Gel Stain (Thermo Fisher Scientific).

Size-exclusion chromatography.

Chromatography was performed as previous described in Chapter II using a Superose 6 Increase 10/300GL column. Each of protein samples, Mms6¹⁻¹¹¹-His (88 μg), Mms6⁷⁵⁻¹³³ (20 μg), Mms6¹⁻⁸⁸ (112 μg), was applied into the column. For protein-protein interaction, a mixture containing two proteins His-MamA and Mms6¹⁻¹¹¹-His, or Mms6⁷⁵⁻¹³³, or Mms6¹⁻⁸⁸, or cytochrome *a*₁-like hemoprotein (control) was incubated for 1 hour at room temperature. All samples were centrifuged at 20,000 × *g* for 10 minutes prior to being injected into the column. Three markers were used, 669-kDa thyroglobulin (bovine thyroid), 220-kDa β-amylase (*Ipomoea batatas*), and 29-kDa carbonic anhydrase (bovine erythrocytes).

Immunoprecipitation assay

The immunoprecipitation assay was performed as described in Chapter II with slight modification. A 200 μl mixture, containing 2 μM His-MamA and 2 μM of each of Mms6 truncated mutants, Mms6¹⁻¹¹¹-His or Mms6¹⁻⁸⁸-His or Mms6⁷⁵⁻¹³³-His, was incubated at 28°C for 1 h. After incubation, 2 μl of the anti-MamA antibody or the normal serum were added to the mixture and incubated for 1 h. Slurry of protein A-Sepharose resin (GE Healthcare Bioscience) was added, and the proteins that

co-precipitated with the protein A-Sepharose resin were analyzed by SDS-PAGE.

Pull-down assay

The poly-His removed MamA obtained as described in Chapter II was used to incubate with Mms6¹⁻¹¹¹-His and with Mms6¹⁻⁸⁸-His. The 50 µl mixtures of 10 µM MamA and 10 µM of each truncated Mms6 proteins were incubated at room temperature for 1 h. Mixtures were added to 15 µl of Ni-NTA agarose resin (QIAGEN), which had been equilibrated with buffer (50 mM NaH₂PO₄ containing 10 mM imidazole and 300 mM NaCl [pH 8.0]) and incubate for 1 h. The resin was then washed five times with 400 µl of the same buffer. The bound proteins were eluted with 15 µl of elution buffer (50 mM NaH₂PO₄ containing 250 mM imidazole, and 300 mM NaCl [pH 8.0]) and the eluted proteins were analyzed by SDS-PAGE. In addition to this, the His-tag removed Mms6⁷⁵⁻¹³³ (Fig. 3-3) was mixed with His-MamA and was precipitated with Ni-NTA agarose resin and the protein-protein interaction was analyzed by SDS-PAGE.

Results and Discussion

Expression, purification and characterization of Mms6 truncated mutants.

I expressed the Mms6¹⁻¹¹¹, which is lacked the C-terminal acidic region, and Mms6¹⁻⁸⁸, which is lacked the putative transmembrane region and the C-terminal acidic region, in *E. coli* (Fig. 3-1). To examine the protein expression, the protein profiles of the soluble fractions and the membrane fractions were analyzed by SDS-PAGE (Fig. 3-2). The 12.5-kDa and 11.0-kDa protein bands corresponded to Mms6¹⁻¹¹¹-His and Mms6¹⁻⁸⁸-His, respectively, were highly expressed but in the different fractions. Mms6¹⁻¹¹¹ was expressed in the membrane fraction, whereas Mms6¹⁻⁸⁸ was expressed in the soluble fraction (Fig. 3-2). The result indicated that the Mms6 is a membrane protein with a single transmembrane helix at a. a. 89 to 111 and the N-terminal domain (a. a. 1 to 88) is soluble. The Mms6¹⁻¹¹¹ and Mms6¹⁻⁸⁸ were purified by Ni²⁺ affinity chromatography from the membrane fraction and from the soluble fraction, respectively, as described in Materials and Methods (Fig. 3-4).

In chapter II, the Mms6¹⁻¹³³ formed oligomer according to the size-exclusion chromatography (SEC) (Fig. 2-11). In order to examine the oligomeric status of Mms6¹⁻¹¹¹, Mms6¹⁻⁸⁸ and Mms6⁷⁵⁻¹³³ proteins, I applied these Mms6 truncated proteins to SEC. The Mms6¹⁻¹¹¹, lacking the C-terminus but maintaining the transmembrane region, eluted with molecular mass over 1,000-kDa, indicating that Mms6¹⁻¹¹¹ forms the oligomer (Fig. 3-5). Also, Mms6⁷⁵⁻¹³³ formed the large oligomer with over 1,000-kDa (Fig. 3-6). In contrast, Mms6¹⁻⁸⁸, lacking the transmembrane region, did not form the large oligomer, and was eluted as a trimer with molecular mass approximate 30.0-kDa (Fig. 3-7). These results suggested that the transmembrane region (a. a. 89 to 111) is needed for oligomerization of Mms6.

Previously, it was reported that the 6.0-kDa Mms6 (Mms6⁷⁵⁻¹³³) was self-assemble to form a large spherical micelle-like oligomer (8, 9). The N-terminal GL-repeat of Mms6⁷⁵⁻¹³³ helps form the micelle-like oligomer (9). The GL-repeat is located in the transmembrane region of Mms6. Therefore, my results were consistent with previous report and showed that the transmembrane region is necessary for self-oligomerization.

Identification of MamA binding site in Mms6

I identified the MamA binding region in Mms6 using three different truncated Mms6 peptides, Mms6¹⁻¹¹¹, Mms6⁷⁵⁻¹³³ and Mms6¹⁻⁸⁸. After mixing and incubating MamA with each of Mms6 truncated mutants, the mixtures of protein samples were applied to SEC. According to SEC, the elution profile of MamA and Mms6¹⁻¹¹¹ mixture showed that two proteins were eluted in the same fraction, indicating the interaction between MamA oligomer and Mms6¹⁻¹¹¹ oligomer (Fig. 3-8). Also, Mms6⁷⁵⁻¹³³ oligomer interacted with MamA oligomer (Fig. 3-9). In contrast, the elution profile of MamA-Mms6¹⁻⁸⁸ mixture showed that Mms6¹⁻⁸⁸ and MamA were separately eluted from the column with molecular masses of ~30.0-kDa and ~500.0-kDa, respectively (Fig. 3-10). Mms6¹⁻⁸⁸ neither formed the large oligomer nor interacted with MamA. Furthermore, the results of the immunoprecipitation (Fig. 3-11) and pull down (Fig. 3-12) assays showed that both Mms6¹⁻¹¹¹ and Mms6⁷⁵⁻¹³³ co-precipitated with MamA, indicating the interactions with MamA. On the other hand, Mms6¹⁻⁸⁸ did not interact with MamA (Fig. 3-11, 12).

Both of MamA and Mms6 contain the hydrophobic regions. The N-terminal putative TPR of MamA (10), and the C-terminal transmembrane region of Mms6 are

hydrophobic parts. Even though these results showed the interaction between MamA and Mms6, the question remains as to whether the interaction is due to the nonspecific hydrophobic binding. To reconcile this, I examined the interaction between MamA and a hydrophobic transmembrane protein, cytochrome a_1 -like hemoprotein purified from *M. magnetotacticum* MS-1 (11, 12) According to SEC, MamA and cytochrome a_1 -like hemoprotein were separately eluted, indicating no interactions (Fig. 3-13). Therefore, the interaction between MamA and Mms6 is not non-specific binding. Moreover, despite a number of hydrophobic magnetosome membrane proteins are contained in the magnetosome protein extracts, only Mms6 was identified as the magnetosome-associated protein among candidates of MamA binding partner by the MamA affinity chromatography. These results showed that MamA-Mms6 interaction is a specific interaction between magnetosome-associated proteins.

These results are giving the idea that the Mms6 transmembrane region interacts with MamA. However, this conflicts with the idea that the Mms6 transmembrane region is embedded in the lipid bilayer of magnetosome membrane. On the other hand, my results suggested that the transmembrane region is needed for oligomerization of Mms6. The oligomerization may be necessary to bind to MamA oligomer. It is possible that the oligomeric state of Mms6 provides an affinity surface which attaches MamA oligomer to magnetosome surface. It is likely that Mms6 oligomer may work as a scaffold in magnetosome membrane that help MamA localizes around magnetosome and function in magnetosome formation.

In this study, I propose a model for a MamA binding site in Mms6 oligomer (Fig. 3-14). Mms6 works as the factor to anchor MamA in magnetosomes. Two types of Mms6, 14.5-kDa Mms6 (Mms6¹⁻¹³³) and 6.0-kDa Mms6 (Mms6⁷⁵⁻¹³³), located on the

magnetosome membrane in roughly equal amounts. The C-terminal part of Mms6 is within the magnetosome vesicle because the C-terminal region of Mms6 contains the putative iron binding site for magnetite synthesis (13, 14). The N-terminal cytosolic part of Mms6 is predicted to provide the binding site which attaches MamA. For the interaction with MamA, two regions of Mms6 are involved in such protein-protein interaction. First, the transmembrane regions are needed for Mms6 self-oligomerization. Second, after Mms6-oligomerization, the cytosolic regions with a. a. 75 to 88 seem to provide a binding site for the interaction with MamA oligomer to form the multiprotein complex in magnetosomes.

Previously, MamA was shown to cover the outside of the magnetosome and to play a role in maintenance processes such as protein sorting or activating magnetosome vesicles (15, 16). My results suggest a direct interaction between MamA and Mms6. Because MamA homogenously surrounds the magnetosomes and are attached to Mms6, these proteins must also be homogenously spaced around the magnetosome as well. This homogeneous localization of Mms6, which controls the magnetite crystal shape, may affect the growth of the magnetite crystals. Therefore, in cells with the *mamA* gene deleted, the magnetite crystals may be altered. This may account for the results shown by Komeili et al. (16) who demonstrated that $\Delta mamA$ AMB-1 cells contained fewer crystals in the magnetosomes vesicles.

There are at least 30 proteins associated with the magnetosome, one of which is MamA, a key protein for the process of constructing the organelle. By proving the fact that Mms6 interacts with MamA, I found a major piece of the puzzle, which allows other researchers to continue the work on MamA and other magnetosome-associated proteins. Over the 40 year history of research on magnetotactic bacteria, a new

protein-protein in magnetosome has been found in this study. This study inspires further studies into the protein-protein interactions in magnetosome to more understand the formation of bacterial magnetic organelles.

References

1. **Braun P, Gingras AC.** 2012. History of protein-protein interactions: from egg-white to complex networks. *Proteomics* **12**: 1478–1498.
2. **Pan W, Xie C, Lv J.** 2012. Screening for the interacting partners of the proteins MamK & MamJ by two-hybrid genomic DNA library of magnetospirillum magneticum AMB-1. *Curr Microbiol* **64**:515–523.
3. **Scheffel A, Schüler D.** 2007. The acidic repetitive domain of the *magnetospirillum gryphiswaldense* MamJ protein displays hypervariability but is not required for magnetosome chain assembly. *J Bacteriol* **189**: 6437–6446.
4. **Carillo MA, Bennet M, Faivre D.** 2013. Interaction of proteins associated with the magnetosome assembly in magnetotactic bacteria as revealed by two-hybrid two-photon excitation fluorescence lifetime imaging microscopy Förster resonance energy transfer. *J Phys Chem B* **117**:14642–14648.
5. **Draper O, Byrne ME, Li Z, Keyhani S, Barrozo JC, Jensen G, Komeili A.** 2011. MamK, a bacterial actin, forms dynamic filaments in vivo that are regulated by the acidic proteins MamJ and LimJ. *Mol. Microbiol.* **82**:342-354.
6. **Komeili A, Li Z, Dianne K, Newman DK, Jensen GJ.** 2006. Magnetosomes Are Cell Membrane Invaginations Organized by the Actin-Like Protein MamK. *Science* **311**: 242-245.
7. **Scheffel A, Gruska M, Faivre D, Linaroudis A, Plitzko JM, Schüler D.** 2006. An acidic protein aligns magnetosomes along a filamentous structure in magnetotactic bacteria. *Nature* **440**:110-114.
8. **Wang L, Prozorov T, Palo PE, Liu X, Vaknin D, Prozorov R, Mallapragada S, Nilsen-Hamilton M.** 2012. Self-assembly and biphasic iron-binding characteristics

- of Mms6, a bacterial protein that promotes the formation of superparamagnetic magnetite nanoparticles of uniform size and shape. *Biomacromolecules* **13**: 98-105.
9. **Feng S, Wang L, Palo P, Liu X, Mallapragada SK, Nilsen-Hamilton M.** 2013. Integrated self-assembly of the Mms6 magnetosome protein to form an iron-responsive structure. *Int. J. Mol. Sci.* **14**:14594-14606.
 10. **Okuda Y, Fukumori Y.** 2001. Expression and characterization of a magnetosome-associated protein, TPR-containing MAM22, in *Escherichia coli*. *FEBS Letters* **491**:169-173.
 11. **Tamegai H, Yamanaka T, Fukumori Y.** 1993. Purification and properties of a 'cytochrome a_1 '-like hemoprotein from magnetotactic bacterium, *Aquaspirillum magnetotacticum*. *Biochimica et Biophysica Acta.* **1158**: 237-243.
 12. **Tanimura Y, Fukumori Y.** 2000. Heme-copper oxidase family structure of *Magnetospirillum magnetotacticum* 'cytochrome a_1 '-like hemoprotein without cytochrome *c* oxidase activity. *J. Inorg. Biochem.* **82**: 73-78.
 13. **Arakaki A, Webb J, Matsunaga T.** 2003. A novel protein tightly bound to bacterial magnetic particles in *Magnetospirillum magneticum* strain AMB-1, *J. Biol. Chem.* **278**:8745-8750.
 14. **Arakaki A, Masuda F, Amemiya Y, Tanaka T, Matsunaga T.** 2010. Control of the morphology and size of magnetite particles with peptides mimicking the Mms6 protein from magnetotactic bacteria. *J. Colloid. Interface Sci.* **343**:65-70.
 15. **Yamamoto D, Taoka A, Uchihashi T, Sasaki H, Watanabe H, Ando T, Fukumori Y.** 2010. Visualization and structural analysis of the bacterial magnetic organelle magnetosome using atomic force microscopy. *Proc. Natl. Acad. Sci. U.S.A.* **107**:9382-9387.

16. **Komeili A, Vali H, Beveridge TJ, Newman DK.** 2004. Magnetosome vesicles are present before magnetite formation, and MamA is required for their activation. Proc. Natl. Acad. Sci. U.S.A. **101**:3839-3844.

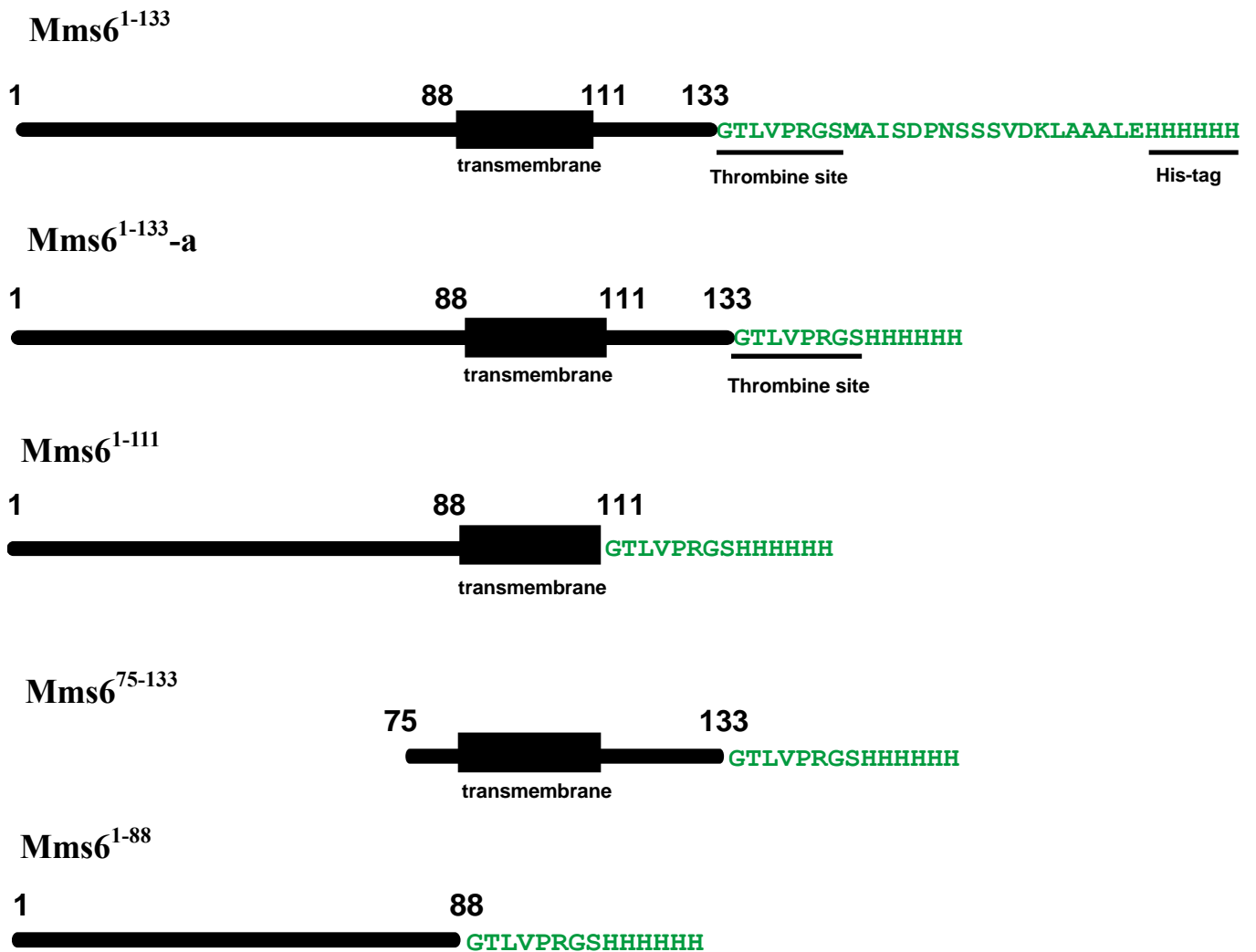


Figure 3-1. Schematic drawing of primary structures of recombinant Mms6 proteins used in this chapter. The Mms6¹⁻¹¹¹ (lacks the C-terminus), Mms6⁷⁵⁻¹³³ (lacks the N-terminus, Chapter II) and Mms6¹⁻⁸⁸ (lacks the C-terminus and transmembrane region) were used.

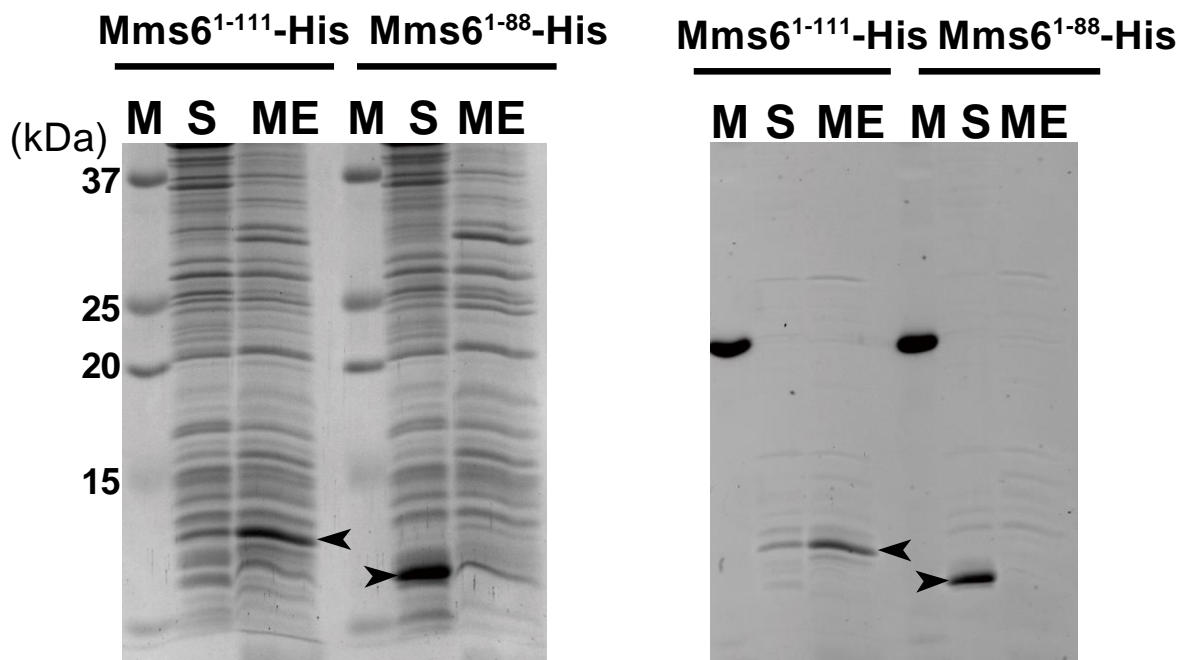


Figure 3-2. Analyses of expressions of truncated Mms6 proteins, Mms6¹⁻¹¹¹-His and Mms6¹⁻⁸⁸-His, by SDS-PAGE. Lane M is protein markers (Precision Plus protein standards; Bio-Rad); lane S is soluble fraction; lane ME is membrane fraction. The Mms6¹⁻¹¹¹ was expressed in the soluble fractions, whereas Mms6¹⁻⁸⁸ was expressed in the membrane fractions. The arrowheads indicated recombinant proteins. The gels were stained with Coomassie Brilliant Blue G-250 (left) and InVision His-tag In-gel (right).

Thrombin cleavage assay

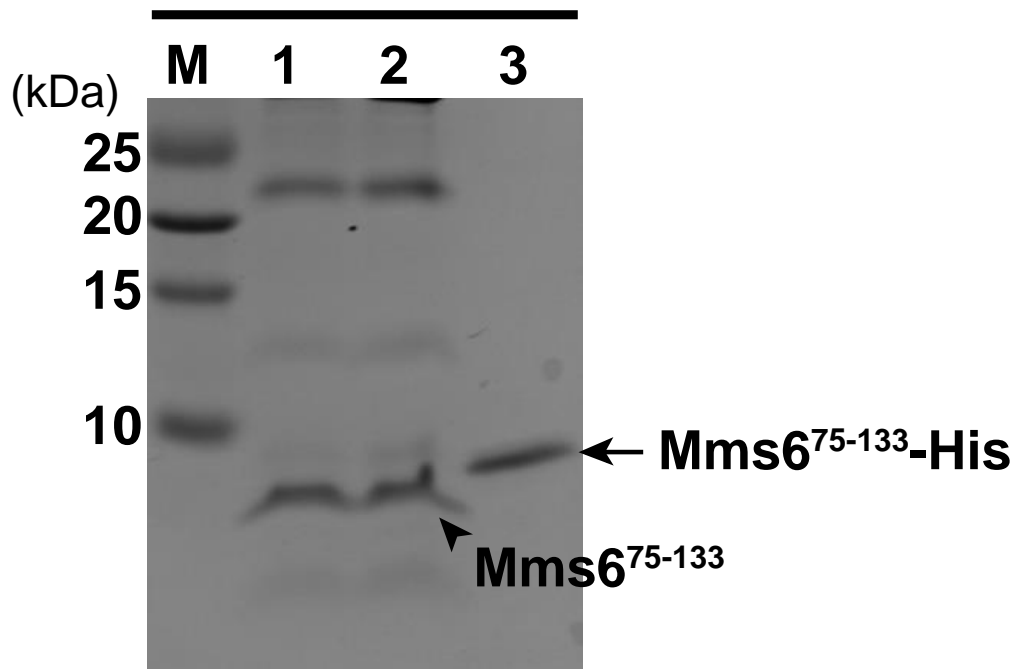


Figure 3-3. Tricine-SDS-PAGE gel profile of thrombin cleavage assay. The poly-His was removed from Mms6⁷⁵⁻¹³³ after the reaction with Biotinylated Thrombin (Novagen) for 16 h (lane 1) or 20 h (lane 2) at room temperature. Lane 3 is the purified Mms6⁷⁵⁻¹³³-His (control); lane M is protein markers. Reaction mixtures were removed the Biotinylated Thrombin by using Streptavidin Agarose. The His-tag removed proteins obtained were used for pull-down assay. Gel was stained with Coomassie Brilliant Blue G-250.

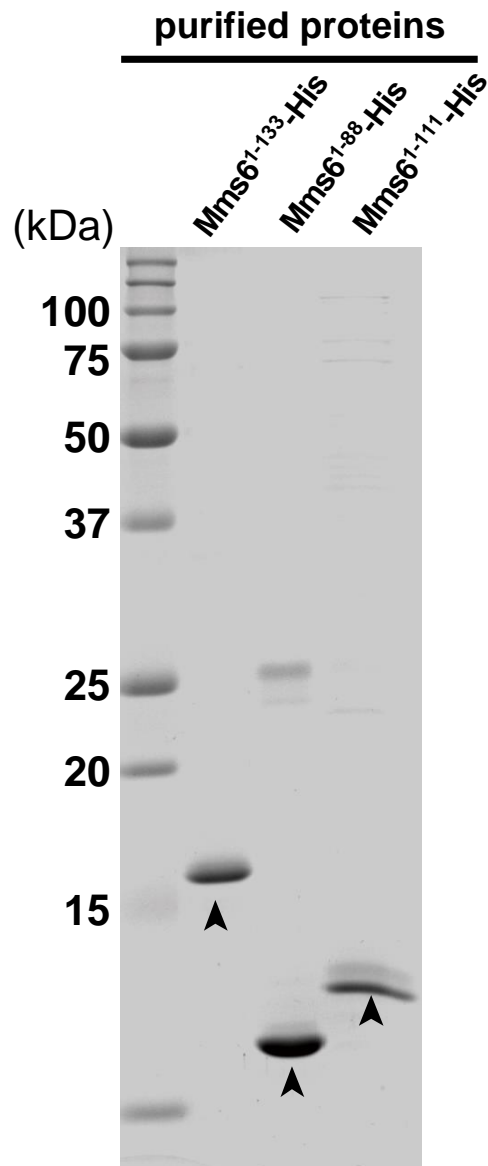


Figure 3-4. Purification of Mms6 proteins using Ni²⁺ affinity chromatography. SDS-PAGE gel profile of purified Mms6 proteins, Mms6¹⁻¹³³ (chapter II), Mms6¹⁻¹¹¹, and Mms6¹⁻⁸⁸. Note that The Mms6¹⁻¹¹¹ was purified from the membrane fraction, whereas Mms6¹⁻⁸⁸ was purified from the soluble fraction. The arrowheads indicated purified Mms6 proteins. The gels were stained with Coomassie Brilliant Blue G-250.

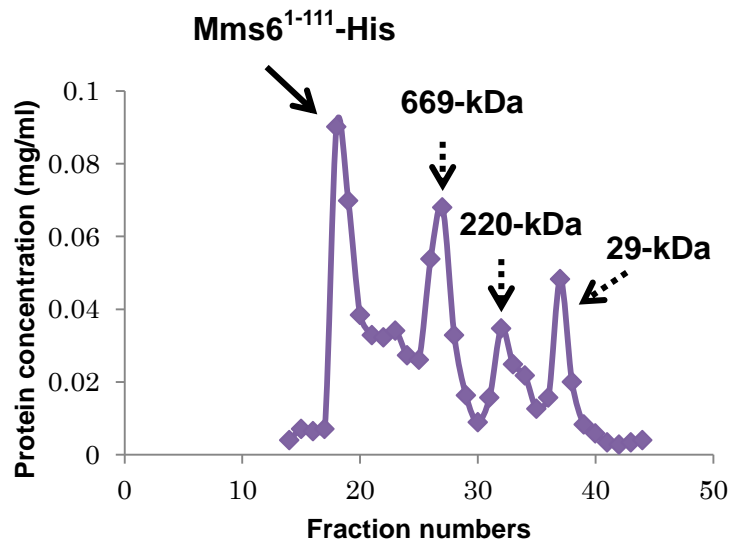
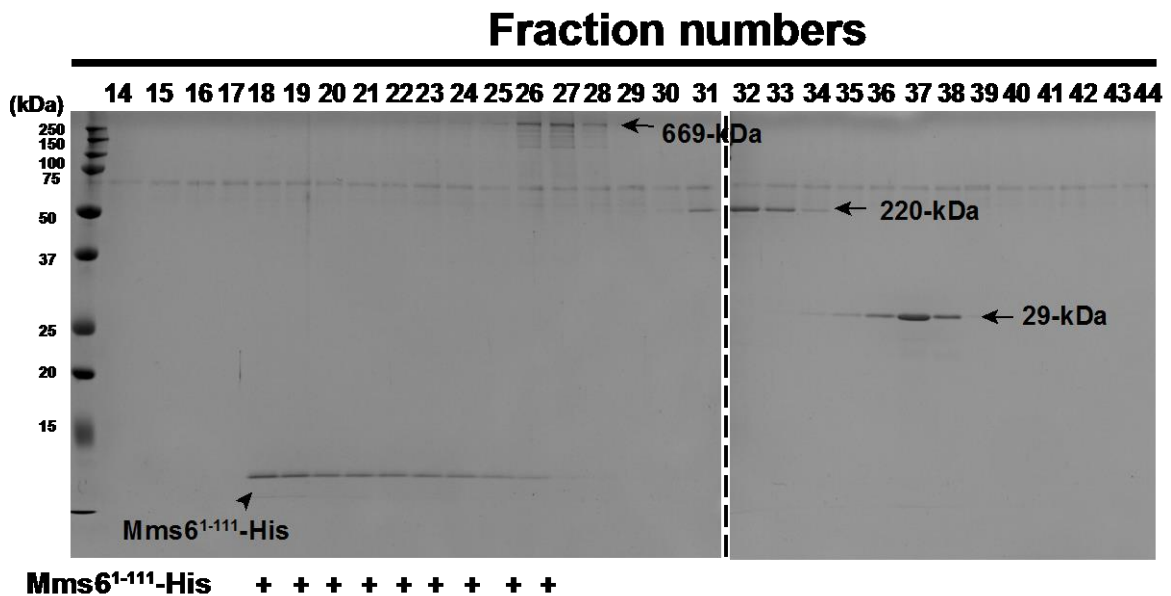
A**B**

Figure 3-5. (A) Elution profile and (B) SDS-PAGE gel profile of Mms6¹⁻¹¹¹-His sample from size exclusion chromatography. Mms6¹⁻¹¹¹ was eluted with molecular mass >1,000-kDa, indicating that Mms6¹⁻¹¹¹ forms oligomer. The bottom parts in SDS-PAGE profiles indicated the presence of proteins in eluted fractions. Three markers were used, 669-kDa thyroglobulin (bovine thyroid), 220-kDa β -amylase (*Ipomoea batatas*), and 29-kDa carbonic anhydrase

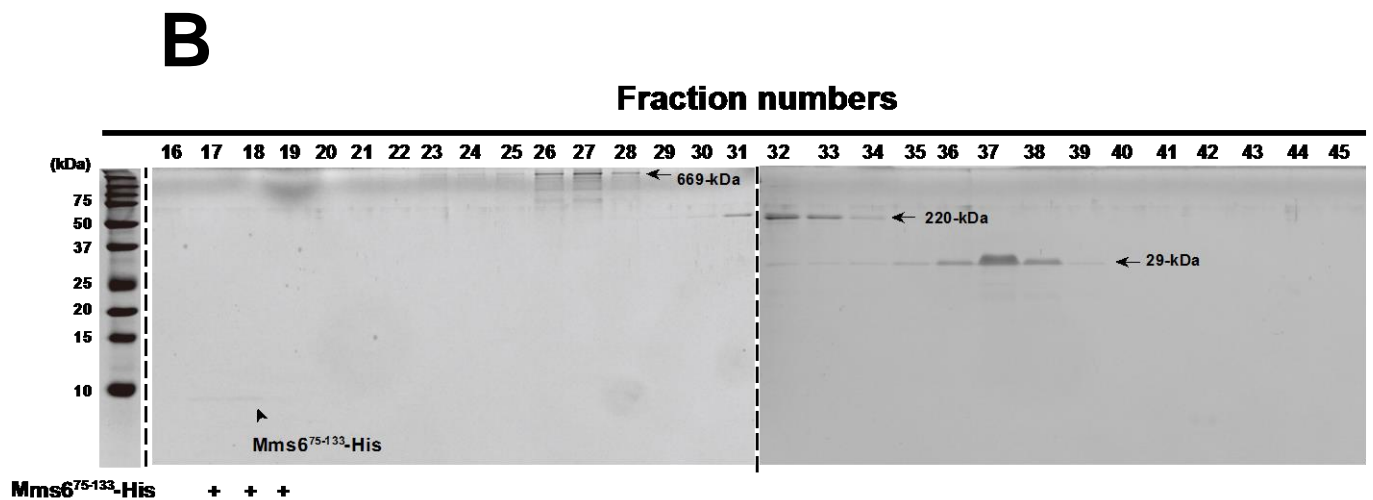
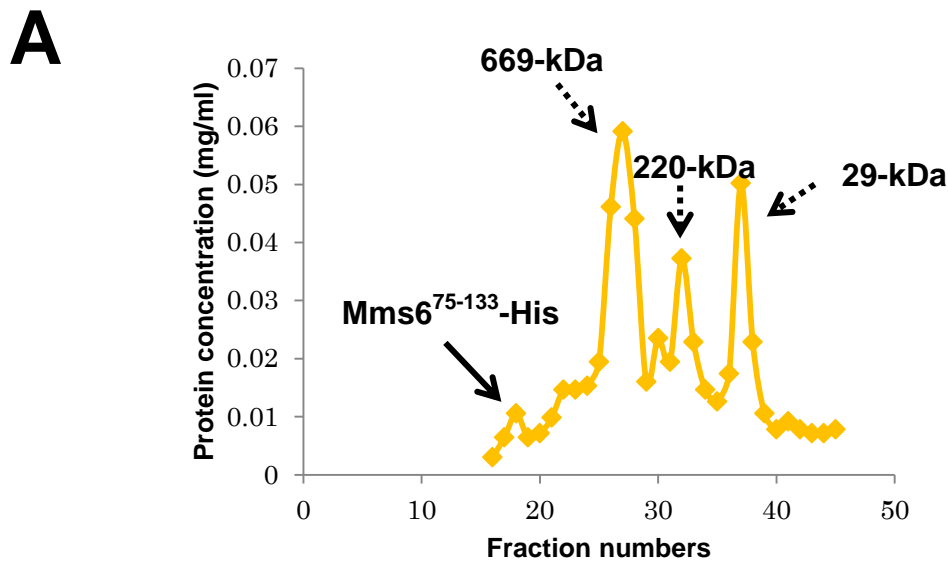


Figure 3-6. (A) Elution profile and (B) Tricine-SDS-PAGE gel profile of Mms6⁷⁵⁻¹³³-His sample from size exclusion chromatography. Mms6¹⁻¹³³ forms larger oligomer with molecular mass >1,000-kDa. The bottom parts in SDS-PAGE profiles indicated the presence of proteins in eluted fractions. Three markers were used, 669-kDa thyroglobulin (bovine thyroid), 220-kDa β -amylase (*Ipomoea batatas*), and 29-kDa carbonic anhydrase (bovine erythrocytes).

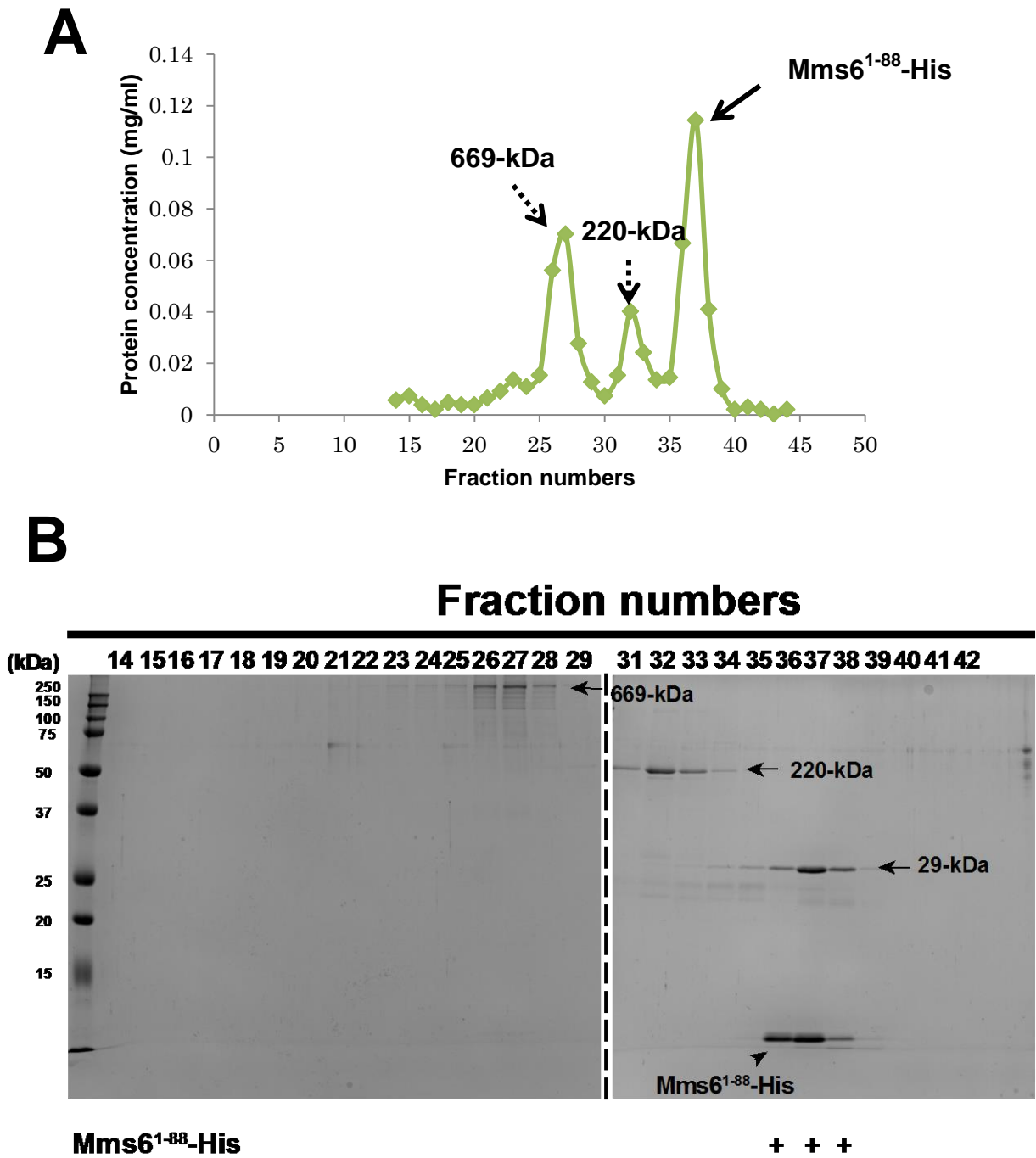


Figure 3-7. (A) The elution profile and (B) SDS-PAGE gel profile of Mms6¹⁻⁸⁸-His sample from size exclusion chromatography. The Mms6¹⁻⁸⁸ was eluted with approximate 30-kDa as the trimer. The bottom parts in SDS-PAGE profiles indicated the presence of proteins in eluted fractions. Three markers were used, 669-kDa thyroglobulin (bovine thyroid), 220-kDa β -amylase (*Ipomoea batatas*), and 29-kDa carbonic anhydrase (bovine erythrocytes).

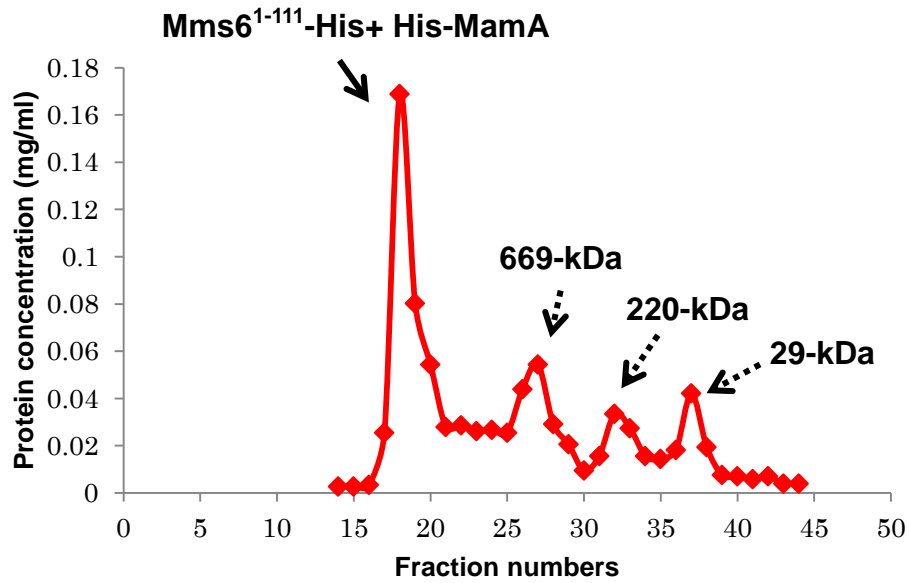
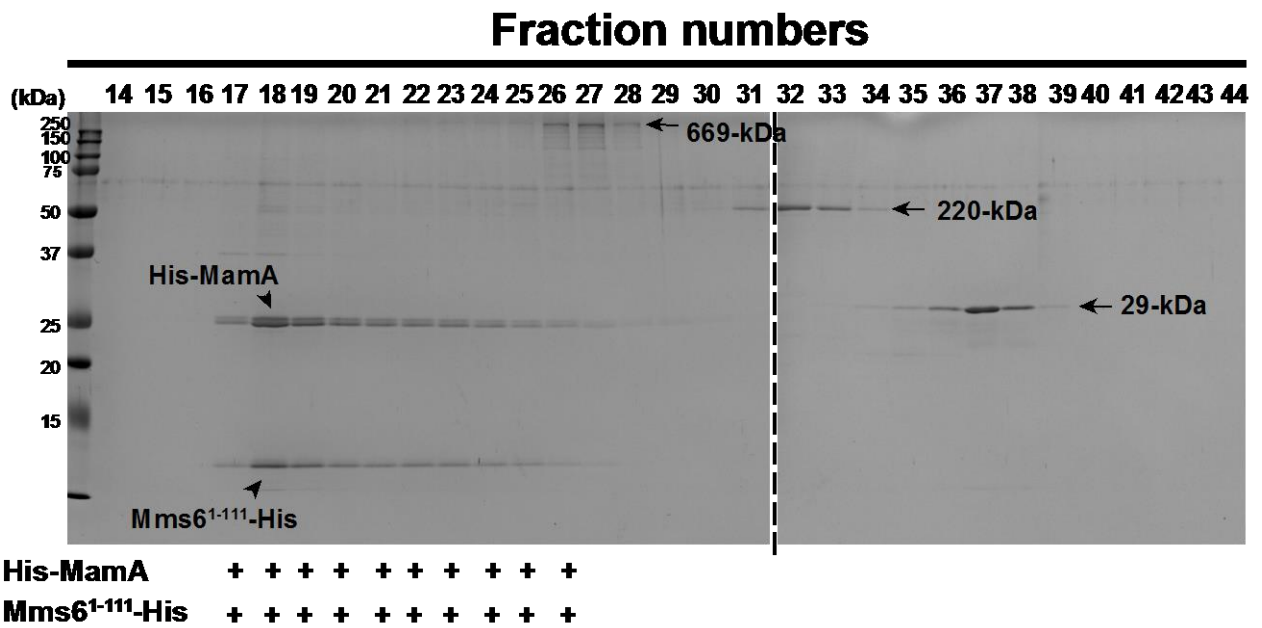
A**B**

Figure 3-8. Analysis of MamA and Mms6¹⁻¹¹¹ interaction by size-exclusion chromatography. The elution profile (A) and SDS-PAGE gel profile (B) of MamA-Mms6¹⁻¹¹¹ mixture. His-MamA and Mms6¹⁻¹¹¹-His were eluted at the same fractions, indicating the interaction between MamA oligomer and Mms6¹⁻¹¹¹ oligomer. The bottom parts in SDS-PAGE profiles indicated the presence of proteins in eluted fractions. Three markers were used, 669-kDa thyroglobulin (bovine thyroid), 220-kDa β -amylase (*Ipomoea batatas*), and 29-kDa carbonic anhydrase (bovine erythrocytes).

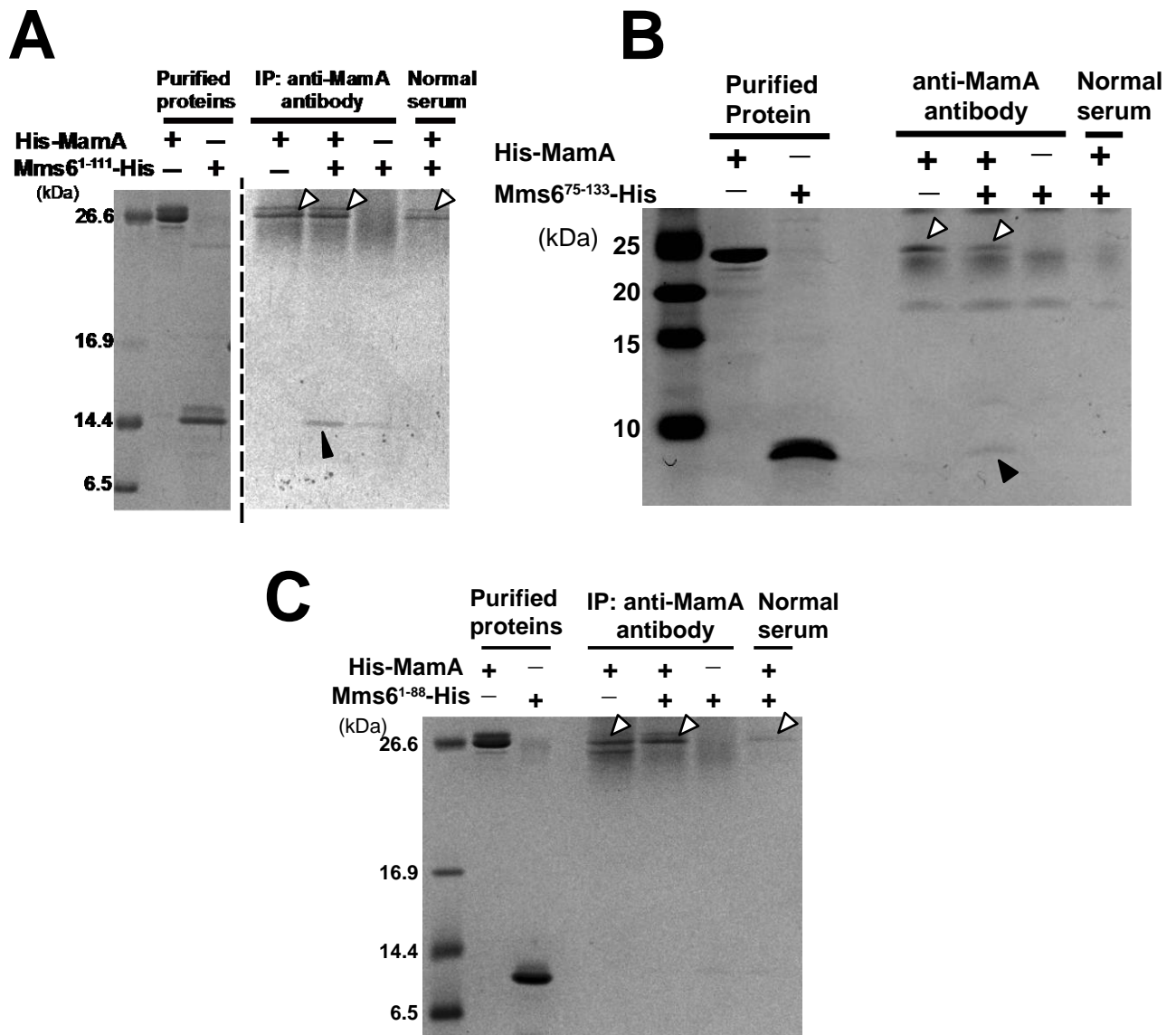


Figure 3-11. SDS-PAGE gel analyses of the immunoprecipitation (IP) assays. Mixtures containing His-MamA and each of Mms6 truncated mutants were precipitated with anti-MamA antibodies. The SDS-PAGE revealed that Mms6¹⁻¹¹¹-His (A) or Mms6⁷⁵⁻¹³³-His (B) co-precipitated with His-MamA, indicating the interactions with MamA. However, Mms6¹⁻⁸⁸-His (C) did not interact with His-MamA. The IP assays indicated that MamA interacts with Mms6¹⁻¹¹¹ and with Mms6⁷⁵⁻¹³³, but not with Mms6¹⁻⁸⁸. The open arrowheads indicate MamA bands and the solid arrowheads indicate Mms6 bands. The gels were stained with Coomassie Brilliant Blue G-250.

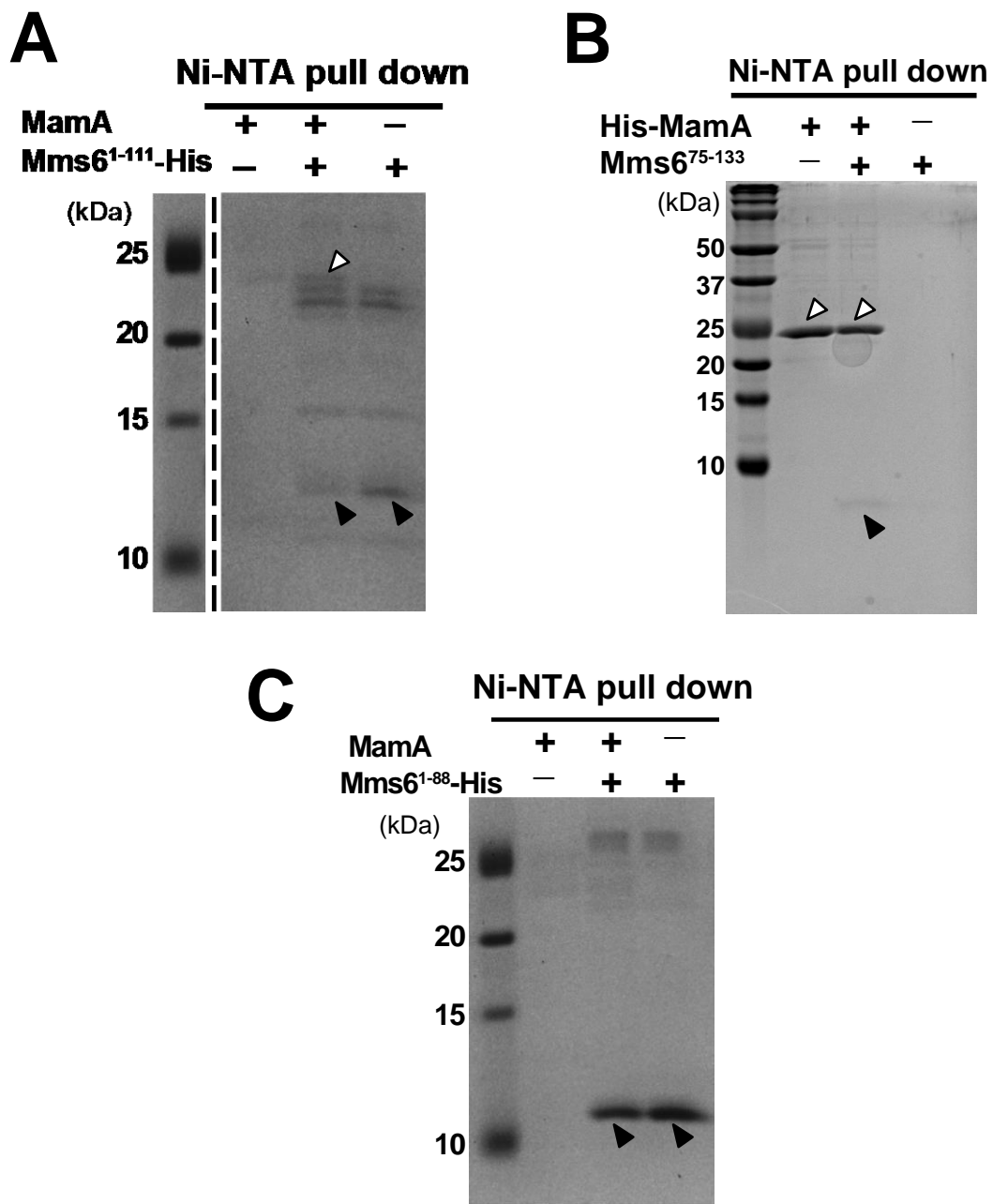
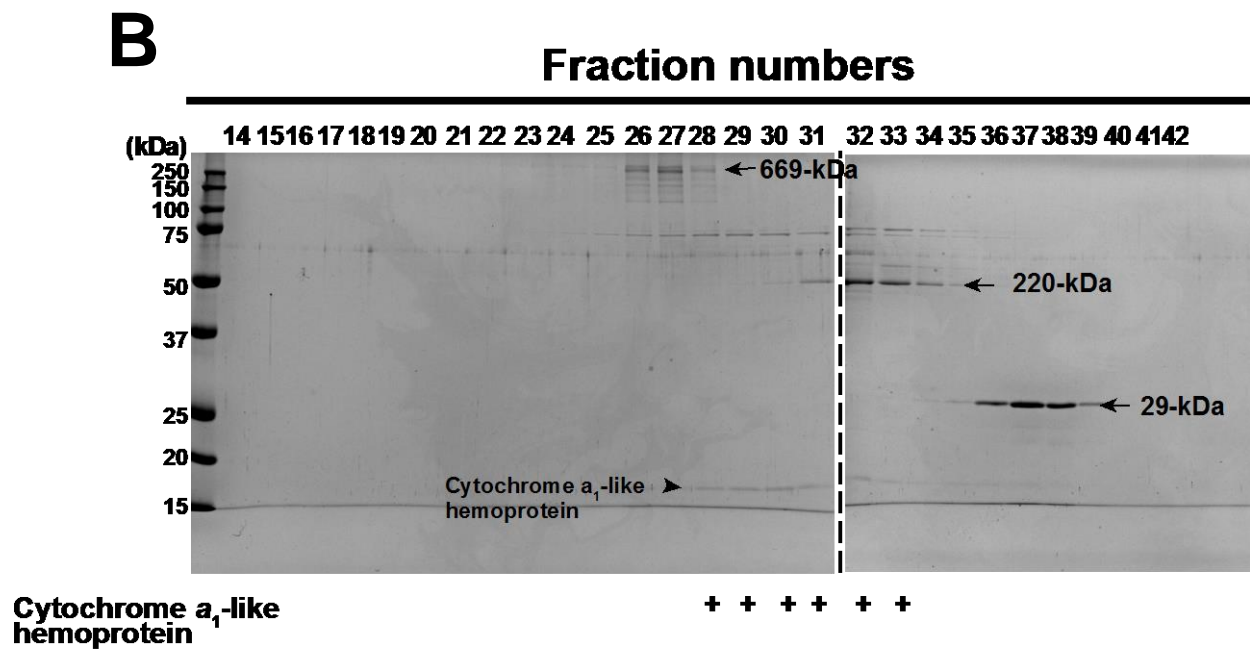
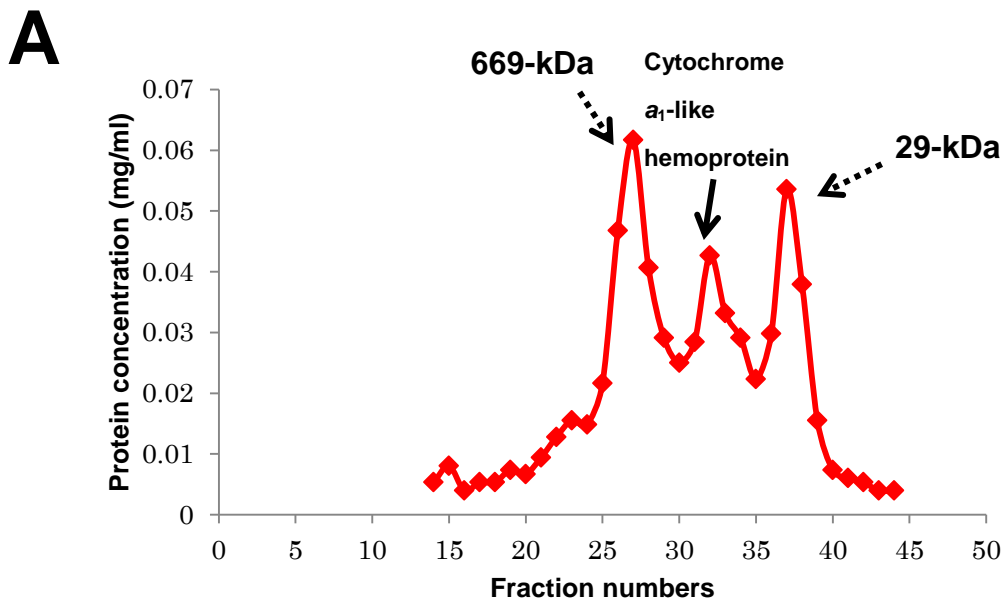


Figure 3-12. SDS-PAGE gels analyses of the Ni-NTA pull down assays. (A) MamA co-precipitated with Mms6¹⁻¹¹¹-His, indicating the MamA-Mms6¹⁻¹¹¹ interaction. (B) Tricine-SDS-PAGE gel analysis showed that Mms6⁷⁵⁻¹³³ interacts with MamA. In contrast, MamA did not co-precipitate with Mms6¹⁻⁸⁸-His, indicating no interaction between MamA and Mms6¹⁻⁸⁸ (C). The open arrowheads indicate MamA bands and the solid arrowheads indicate Mms6 bands. The gels were stained with Coomassie Brilliant Blue G-250.



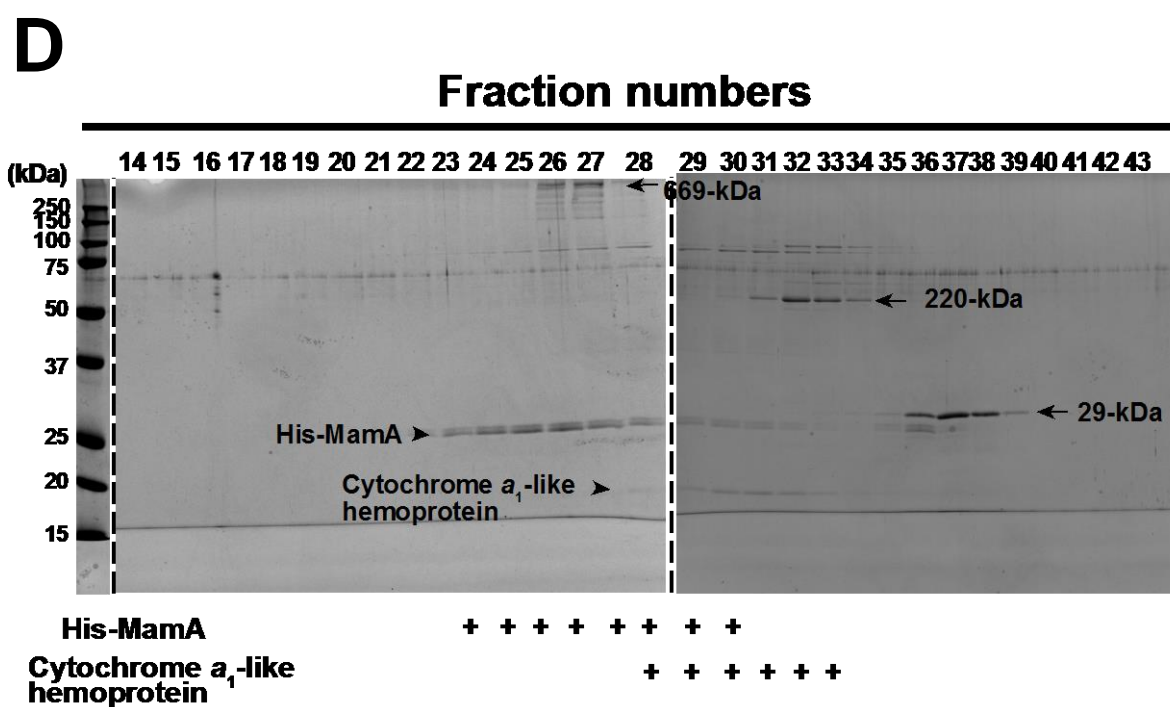
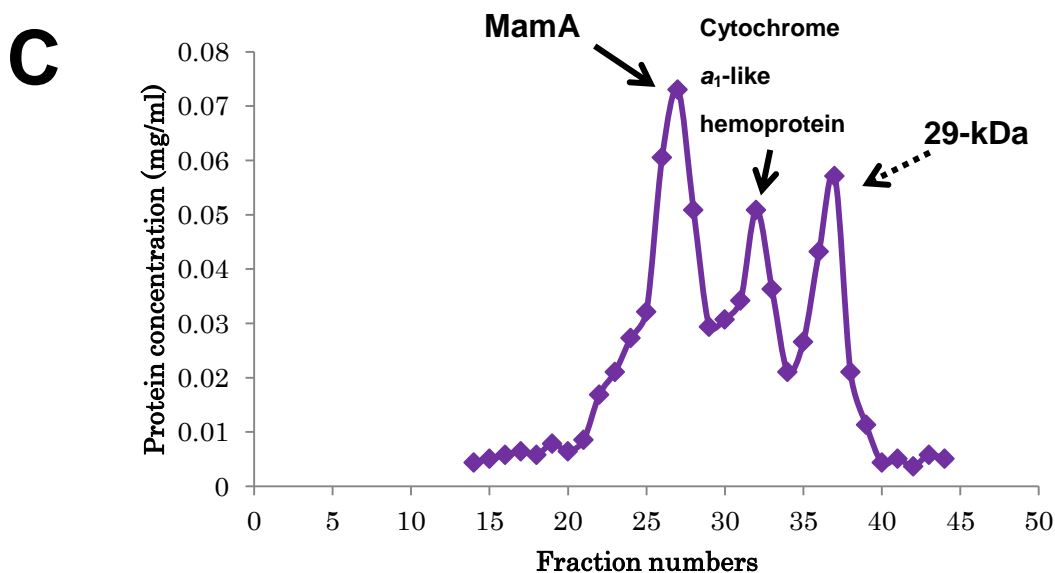


Figure 3-13. Analysis of MamA and cytochrome a_1 -like hemoprotein interaction by size-exclusion chromatography. (A) The elution profile and (B) SDS-PAGE gel profile of cytochrome a_1 -like hemoprotein fractions. (C) The elution profile and (D) SDS-PAGE profile of the sample containing His-MamA and cytochrome a_1 -like hemoprotein. Note that there is no interaction between His-MamA and cytochrome a_1 -like hemoprotein. The bottom parts in SDS-PAGE profiles indicate the presence of proteins in eluted fractions. Three markers were used, 669-kDa thyroglobulin (bovine thyroid), 220-kDa α -amylase (*Ipomoea batatas*), and 29-kDa carbonic anhydrase (bovine erythrocytes).

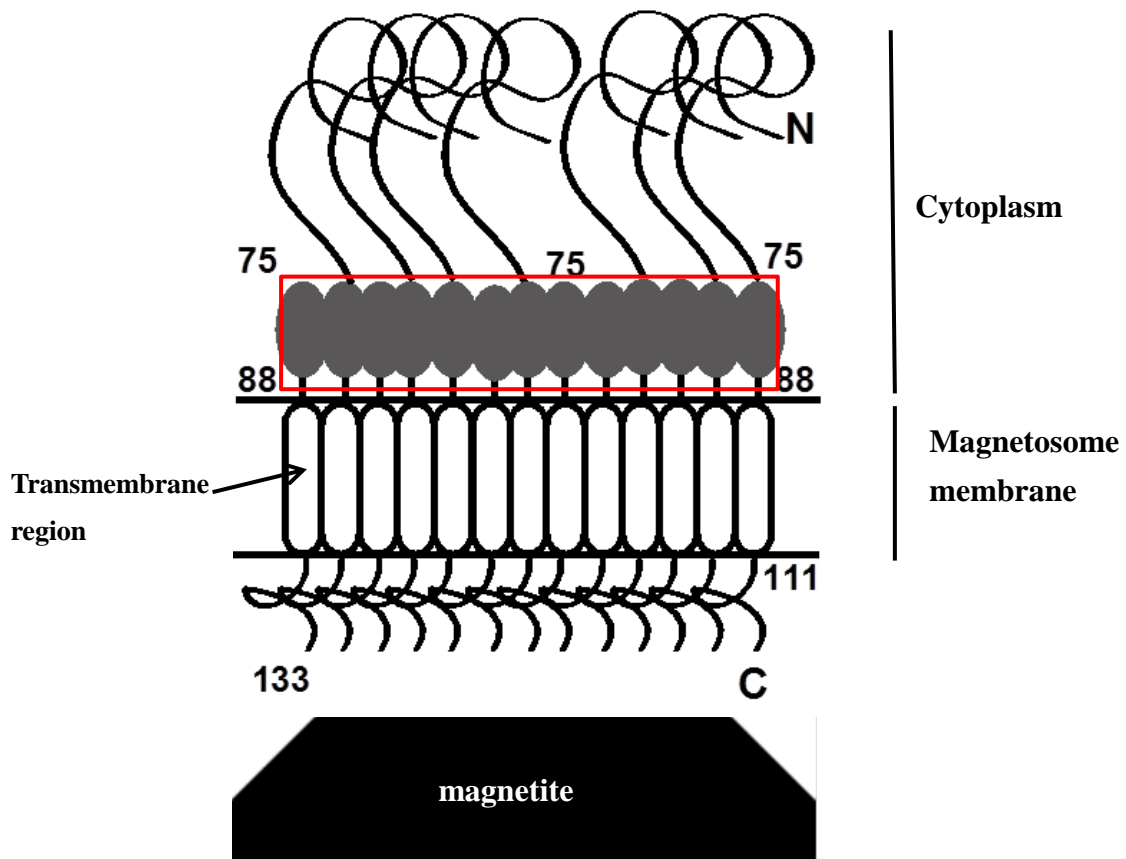


Figure 3-14. Schematic model for the Mms6 oligomerization which provides the MamA binding site. Two types of Mms6, the 14.5-kDa Mms6¹⁻¹³³ and the 6.0-kDa Mms6⁷⁵⁻¹³³, exit in magnetosome membrane in roughly equal amounts. The C-terminal parts of Mms6 are inside the magnetosome vesicle because the C-terminal region of Mms6 contains the putative iron binding site for magnetite synthesis (13, 14). Mms6 proteins interact with each other by transmembrane region to form the large oligomer in magnetosome membrane. After oligomerization, the N-terminal parts of Mms6 (a. a. 75 to 88) in the cytosol are predicted to provide the binding site which attaches MamA oligomer in magnetosome. The red box indicates the MamA binding site of Mms6 oligomer.

Table 3-1. Bacterial strains and plasmids used in this study

Strains and plasmids	Description	Source or reference
<i>Strains</i>		
<i>E. coli</i> XL-1 blue MRF ⁺	$\Delta(mcrA)183 \Delta(mcrCB-hsdSMR-mrr)173$ <i>endA1 supE44 thi-1 recA1 gryA96 relA1 lac</i> [F', <i>proAB</i> , <i>laqI</i> ^{qZ} Δ M15, Tn10(Tet ^R)]	Stratagene
<i>E. coli</i> BL21(DE3)	<i>hsdS gal</i> (λ CIts857 <i>ind1 Sam7 nin5 lacUV5-T7</i> <i>gen I</i>)	Novagen
<i>Plasmids</i>		
pET29b-mms6 ¹⁻¹³³ -a	pET29b carrying <i>mms6</i> ¹⁻¹³³ gene from AMB-1	This study
pET29b-mms6 ¹⁻¹¹¹	pET29b carrying <i>mms6</i> ¹⁻¹¹¹ gene from AMB-1	This study
pET29b-mms6 ¹⁻⁸⁸	pET29b carrying <i>mms6</i> ¹⁻⁸⁸ gene from AMB-1	This study

Table 3-2. Primers used in this study.

Primer name	Sequence (5'-3')
FW -mms6-a	5'-CACCACCACCACCACCACTGAG-3'
RV -mms6-a	5'-GGAACCGCGTGGCACCAGGGTACC-3'
FW -mms61-111	5'-GGTACCCTGGTGCCACGCGGTTCC-3'
RV -mms61-111	5'-ATACGCGTAAACCGCCCCGGCG-3'
FW-mms6 1-88	5'-GGTACCCTGGTGCCACGCGGTTCC-3'
RV-mms61-88	5'-CAGACCGAGGCCAGCCCCTTAC-3'

Conclusions

The outcome of my research is two-fold:

1. I specified the binding partner of MamA. In this study, I convincingly showed the interaction between MamA and Mms6. This study, for the first time, described the exit of 14.5-kDa Mms6 (Mms6¹⁻¹³³) in magnetosome. Also, a new role of Mms6 in magnetosome membrane that anchors MamA has been proposed in this study.
2. I determined that the transmembrane region of Mms6 function in Mms6 self-assembly to form large oligomer. The oligomerization of Mms6 may be necessary for the interaction with MamA.

Moreover, an important next step remains to as *in vivo* studies of the MamA-Mms6 interaction. Specifically, the knowledge to as MamA localization in the *mms6* gene deletion mutant AMB-1 still remains undermined and need to be studied in the future.

Acknowledgements

I would first like to express my sincere gratitude to Professor Yoshihiro Fukumori, Kanazawa University for suggesting this study and supporting throughout my study in Japan. I would also like to thank to Assistant Professor Azuma Taoka, Kanazawa University for helpful advices, valuable teaching and discussions to all my research. I am grateful Associate Professor Massaki Kanemori, Kanazawa University for insightful comments and encouragements.

I also appreciate much Dr. Zachery Oestreicher (Ohio State University, the United State of America) for supporting and developing my research. My sincere thanks also go to Professor Hiroshi Endoh for his supports to me in Kanazawa University. I thank to members of Fukumori laboratory for their helps and discussions in my research as well as my daily life in Japan.

I would like to thank to my family for spiritual support throughout my life. Finally, I sincerely acknowledge the Mekong Camau120 Project, Vietnam for providing me a chance to study in Japan.